



HAL
open science

Data-driven polynomial chaos expansions for machine learning regression

E Torre, S. Marelli, P Embrechts, B. Sudret

► **To cite this version:**

E Torre, S. Marelli, P Embrechts, B. Sudret. Data-driven polynomial chaos expansions for machine learning regression. 2018. hal-01893177

HAL Id: hal-01893177

<https://hal.science/hal-01893177>

Preprint submitted on 11 Oct 2018

HAL is a multi-disciplinary open access archive for the deposit and dissemination of scientific research documents, whether they are published or not. The documents may come from teaching and research institutions in France or abroad, or from public or private research centers.

L'archive ouverte pluridisciplinaire **HAL**, est destinée au dépôt et à la diffusion de documents scientifiques de niveau recherche, publiés ou non, émanant des établissements d'enseignement et de recherche français ou étrangers, des laboratoires publics ou privés.

DATA-DRIVEN POLYNOMIAL CHAOS EXPANSION FOR MACHINE LEARNING REGRESSION

E. Torre, S. Marelli, P. Embrechts, B. Sudret



Data Sheet

Journal:

Report Ref.: RSUQ-2018-005

Arxiv Ref.: <http://arxiv.org/abs/1808.03216> - [stat.CO] [stat.ML]

DOI:

Date submitted: 11 June 2018

Date accepted: -

Data-driven polynomial chaos expansion for machine learning regression

E. Torre, S. Marelli, P. Embrechts, B. Sudret

Abstract

We present a regression technique for data driven problems based on polynomial chaos expansion (PCE). PCE is a popular technique in the field of uncertainty quantification (UQ), where it is typically used to replace a runnable but expensive computational model subject to random inputs with an inexpensive-to-evaluate polynomial function. The metamodel obtained enables a reliable estimation of the statistics of the output, provided that a suitable probabilistic model of the input is available.

In classical machine learning (ML) regression settings, however, the system is only known through observations of its inputs and output, and the interest lies in obtaining accurate pointwise predictions of the latter. Here, we show that a PCE metamodel purely trained on data can yield pointwise predictions whose accuracy is comparable to that of other ML regression models, such as neural networks and support vector machines. The comparisons are performed on benchmark datasets available from the literature. The methodology also enables the quantification of the output uncertainties and is robust to noise. Furthermore, it enjoys additional desirable properties, such as good performance for small training sets and simplicity of construction, with only little parameter tuning required. In the presence of statistically dependent inputs, we investigate two ways to build the PCE, and show through simulations that one approach is superior to the other in the stated settings.

Keywords: sparse polynomial chaos expansions, machine learning, regression, uncertainty quantification, copulas.

1 Introduction

Machine learning (ML) is increasingly used today to make predictions of system responses and to aid or guide decision making. Given a d -dimensional input vector \mathbf{X} to a system and the corresponding q -dimensional output vector \mathbf{Y} , data-driven ML algorithms establish a map $\mathcal{M}: \mathbf{X} \mapsto \mathbf{Y}$ on the basis of an available sample set $\mathcal{X} = \{\mathbf{x}^{(1)}, \dots, \mathbf{x}^{(n)}\}$ of input observations and of the corresponding output values $\mathcal{Y} = \{\mathbf{y}^{(1)}, \dots, \mathbf{y}^{(n)}\}$, where $\mathbf{y}^{(i)} =$

$\mathcal{M}(\mathbf{x}^{(i)})$. In classification tasks, the output \mathbf{Y} is discrete, that is, it can take at most a countable number of different values (the class *labels*). In regression tasks, which this paper is concerned with, the output \mathbf{Y} takes continuous values. Regression techniques include linear regression, neural networks (NN), kernel methods (such as Gaussian processes, GP), sparse kernel machines (such as support vector machines, SVM), graphical models (such as Bayesian networks and Markov random fields), and others. A comprehensive overview of these methods can be found in Bishop (2009) and in Witten et al. (2016).

Current research on ML algorithms focuses on various open issues. First, there is an increasing interest towards problems where the inputs to the system, and as a consequence the system's response, are uncertain (see, *e.g.*, Chan and Elsheikh (2018); Kasiviswanathan et al. (2016); Mentch and Hooker (2016)). Properly accounting for both aleatory and epistemic input uncertainties allows one to estimate the response statistics. Second, novel methods are sought to better automatize the tuning of hyperparameters, which several ML methods are highly sensitive to (Snoek et al., 2012). Third, the paucity of data in specific problems calls for models that can be effectively trained on few observations only (Forman and Cohen, 2004). Finally, complex models, while possibly yielding accurate predictions, are often difficult if not impossible to interpret.

This manuscript revisits polynomial chaos expansions (PCE), a well established meta-modelling technique in uncertainty quantification (UQ), as a statistical ML regression algorithm (Vapnik, 1995) that can deal with these challenges (Sudret et al., 2015). UQ classically deals with problems where \mathbf{X} is uncertain, and is therefore modelled as a random vector. As a consequence, $\mathbf{Y} = \mathcal{M}(\mathbf{X})$ is also uncertain, but its statistics are unknown and have to be estimated. Differently from ML, in UQ the model \mathcal{M} is typically available (*e.g.*, as a finite element code), and can be computed pointwise. However, \mathcal{M} is often a computationally expensive black-box model, so that a Monte Carlo approach to estimate the statistics of \mathbf{Y} (generate a large input sample set \mathcal{X} to obtain a large output sample set $\mathcal{Y} = \{\mathcal{M}(\mathbf{x}), \mathbf{x} \in \mathcal{X}\}$) is not feasible. PCE is a UQ spectral technique that is used in these settings to express \mathbf{Y} as a polynomial function of \mathbf{X} . PCE thereby allows one to replace the original computational model \mathcal{M} with an inexpensive-to-run but accurate metamodel. The metamodel can be used to derive, for instance, estimates of various statistics of \mathbf{Y} , such as its moments or its sensitivity to different components of \mathbf{X} (Saltelli et al., 2000), in a computationally efficient way. Recently, we established a general framework to perform UQ (including PCE metamodeling) in the presence of complex input dependencies modelled through copulas (Torre et al., 2017).

Here, we re-establish PCE in a purely data-driven ML setup, where the goal is to obtain a model that can predict the response \mathbf{Y} of a system given its inputs \mathbf{X} . For simplicity, we consider the case where \mathbf{Y} is a scalar random variable Y . The generalisation to multivariate outputs is straightforward. In the setup of interest here, no computational model \mathcal{M} is

available, but only a set $(\mathcal{X}, \mathcal{Y})$ of input values and corresponding responses. \mathcal{X} and \mathcal{Y} are considered to be (possibly noisy) realisations of \mathbf{X} and Y , the true relationship between which is deterministic but unknown.

After recalling the underlying theory (Section 2), we first show by means of simulation that data-driven PCE delivers accurate pointwise predictions (Section 3). In addition, PCE also enables a reliable estimation of the statistics of the response (such as its moments and PDF), thus enabling uncertainty quantification of the predictions being made. Dependencies among the input variables are effectively modelled by copula functions, purely inferred from the data as well. The approach is shown to be robust to noise in the data, and to work well also in the presence of small training sets. In Section 4, we further apply PCE to real data previously analyzed by other authors with different NN and/or SVM algorithms, where it achieves a comparable performance. Importantly, the construction of the PCE metamodel does not rely on fine tuning of critical hyper-parameters. This and other desirable features of the PCE modelling framework are discussed in Section 5.

2 Methods

2.1 Measures of accuracy

Before introducing PCE, which is a popular metamodeling technique in UQ, as an ML technique used to make pointwise predictions, it is important to clarify the distinction between the error types that UQ and ML typically aim at minimizing.

ML algorithms are generally used to predict, for any *given* input, the corresponding output of the system. Their performance is assessed in terms of the distance of the prediction from the actual system response, calculated for each input and averaged over a large number of (ideally, all) possible inputs. A common error measure in this sense is the mean absolute error (MAE). For a regression model \mathcal{M} trained on a training data set $(\mathcal{X}', \mathcal{Y}')$, the MAE is typically evaluated over a validation data set $(\mathcal{X}'', \mathcal{Y}'')$ of size n'' by

$$\text{MAE} = \frac{1}{n''} \sum_{(\mathbf{x}, y) \in (\mathcal{X}'', \mathcal{Y}'')} |y - \mathcal{M}(\mathbf{x})|. \quad (1)$$

The associated relative error considers point by point the ratio between the absolute error and the actual response, *i.e.*,

$$\text{rMAE} = \frac{1}{n} \sum_{(\hat{\mathbf{x}}, \hat{y}) \in (\mathcal{X}, \mathcal{Y})} \left| \frac{\hat{y} - \mathcal{M}(\hat{\mathbf{x}})}{\hat{y}} \right| = \frac{1}{n} \sum_{(\hat{\mathbf{x}}, \hat{y}) \in (\mathcal{X}, \mathcal{Y})} \left| 1 - \frac{\mathcal{M}(\hat{\mathbf{x}})}{\hat{y}} \right|, \quad (2)$$

which is well defined if $\hat{y} \neq 0$ for all $\hat{y} \in \mathcal{Y}$.

PCE is instead typically used to draw accurate estimates of various statistics of the output – such as its moments, its PDF, confidence intervals – given a probabilistic model $f_{\mathbf{X}}$ of an uncertain input. The relative error associated to the estimates $\hat{\mu}_Y$ of μ_Y and $\hat{\sigma}_Y$ of σ_Y is

often quantified by

$$\left|1 - \frac{\hat{\mu}_Y}{\mu_Y}\right|, \quad \left|1 - \frac{\hat{\sigma}_Y}{\sigma_Y}\right|, \quad (3)$$

provided that $\mu_Y \neq 0$ and $\sigma_Y \neq 0$.

A popular measure of the error made on the full response PDF f_Y is the Kullback-Leibler divergence

$$\Delta_{\text{KL}}(\hat{f}_Y|f_Y) = \int_y \log \left(\frac{\hat{f}_Y(y)}{f_Y(y)} \right) f_Y(y) dy, \quad (4)$$

which quantifies the average difference between the logarithms of the predicted and of the true PDFs.

Provided a suitable model $f_{\mathbf{X}}$ of the joint PDF of the input, PCE is known to converge (in the sense that the error on the mentioned output statistics decreases) very rapidly as the size of the training set increases, compared for instance to Monte-Carlo sampling (Puig et al., 2002; Todor and Schwab, 2007; Ernst et al., 2012). This happens because PCE, which is a spectral method, efficiently propagates the probabilistic information delivered by the input model $f_{\mathbf{X}}$ to the output. Nevertheless, this does not necessarily imply a similarly rapid pointwise convergence of the error, which remains to be demonstrated. For a discussion of various types of convergence, see Ernst et al. (2012) and references therein.

2.2 Data-driven settings

PCE is designed to build an inexpensive-to-evaluate analytical model $Y_{PC} = \mathcal{M}_{PC}(\mathbf{X})$ mapping an input random vector \mathbf{X} onto an output random variable Y (Ghanem and Spanos, 1990; Xiu and Karniadakis, 2002). PCE assumes that an unknown deterministic map $\mathcal{M} : \mathbb{R}^d \rightarrow \mathbb{R}$ exists, such that $Y = \mathcal{M}(\mathbf{X})$. Y is additionally assumed to have finite variance: $\mathbb{V}(Y) = \int_{\mathbb{R}^d} \mathcal{M}^2(\mathbf{x}) f_{\mathbf{X}}(\mathbf{x}) d\mathbf{x} < +\infty$. Under the further assumption that each X_i has finite moments of all orders (Ernst et al., 2012), the space of square integrable functions with respect to $f_{\mathbf{X}}(\cdot)$ admits a basis $\{\Psi_{\alpha}(\cdot), \alpha \in \mathbb{N}^d\}$ of polynomials orthonormal to each other with respect to the probability measure $f_{\mathbf{X}}$, *i.e.*, such that

$$\int_{\mathbb{R}^d} \Psi_{\alpha}(\mathbf{x}) \Psi_{\beta}(\mathbf{x}) f_{\mathbf{X}}(\mathbf{x}) d\mathbf{x} = \delta_{\alpha\beta}. \quad (5)$$

Here, $\delta_{\alpha\beta}$ is the Kroencker delta symbol. The element α_i of the multi-index $\alpha \in \mathbb{N}^d$ indicates the degree of Ψ_{α} in the i -th variable, $i = 1, \dots, d$. Ψ_{α} has a total degree given by $|\alpha| = \sum_i \alpha_i$.

Thus, Y admits the spectral representation

$$Y(\mathbf{X}) = \sum_{\alpha \in \mathbb{N}^d} y_{\alpha} \Psi_{\alpha}(\mathbf{X}). \quad (6)$$

The goal of PCE is to determine the coefficients y_{α} of the expansion, truncated at some polynomial order, given an initial set $(\mathcal{X}, \mathcal{Y})$ of observations (the *training set* or *experimental design*). In some engineering applications the model $\mathcal{M}(\cdot)$ is directly available (*e.g.*, as a

finite element model) but computationally expensive to evaluate: in these cases, PCE is used as a surrogate to replace the true model with an inexpensive-to-evaluate metamodel. In the standard ML settings considered here, conversely, $\mathcal{M}(\cdot)$ is unknown and has to be modelled solely on the basis of available observations $(\mathcal{X}, \mathcal{Y})$. The primary goal of this paper is to show that the accuracy of a PCE metamodel built purely on $(\mathcal{X}, \mathcal{Y})$ can compete with that of state-of-the-art machine learning regression models, while requiring little parameter tuning and in some cases offering additional advantages.

2.3 PCE for independent inputs

In this section, we assume that the input random vector \mathbf{X} has statistically independent components. The PCE basis is built from the tensor product of univariate orthogonal polynomials. The case of inputs with dependent components is discussed later in Section 2.4.

2.3.1 Orthogonalization for independent inputs

When \mathbf{X} has independent components, the Ψ_{α} can be obtained as the tensor product of d univariate polynomials,

$$\Psi_{\alpha}(\mathbf{x}) = \prod_{i=1}^d \phi_{\alpha_i}^{(i)}(x_i), \quad (7)$$

where each $\phi_{\alpha_i}^{(i)}(x_i)$ is the element of degree α of a basis of univariate polynomials orthonormal with respect to the marginals f_i of \mathbf{X} , that is, such that

$$\int_{\mathbb{R}} \phi_{\alpha_i}^{(i)}(\omega) \phi_{\beta_i}^{(i)}(\omega) f_i(\omega) d\omega = \delta_{\alpha_i \beta_i}. \quad (8)$$

The problem of building a basis of mutually orthonormal multivariate polynomials with respect to $f_{\mathbf{X}}$ hence becomes the problem of building d bases of mutually orthonormal univariate polynomials, each with respect to a marginal f_i . The d bases can be built independently.

2.3.2 Specification of the marginals and arbitrary PCE

The construction of the polynomial basis requires a model of the marginal input distributions. Families of univariate orthonormal polynomials associated to classical continuous distributions are described in Xiu and Karniadakis (2002). An input variable X_i with a different distribution F_i (continuous, strictly increasing) may be transformed to a random variable \tilde{X}_i with distribution Φ belonging to one of the classical families by the transformation

$$\tilde{X}_i = \Phi^{-1}(F_i(X_i)). \quad (9)$$

This relation offers a first possible approach to build the PCE of Y for inputs \mathbf{X} with generic continuous marginals F_i : transform \mathbf{X} into $\tilde{\mathbf{X}}$ through (9), and then build a PCE of Y in terms of $\tilde{\mathbf{X}}$. The PCE has to be trained on $(\tilde{\mathcal{X}}, \mathcal{Y})$, where $\tilde{\mathcal{X}}$ is obtained from \mathcal{X} using (9).

Alternatively, it is possible to directly construct a basis of orthonormal polynomials with respect to F_i by Stiltjes or Gram-Schmidt orthogonalization (Soize and Ghanem, 2004; Wan and Karniadakis, 2006). The polynomial chaos representation for arbitrary distributions is known as arbitrary PCE. In practice, performing arbitrary PCE on the original input \mathbf{X} is preferable to building the PCE on inputs transformed via (9). Indeed, the latter is usually a highly non-linear transformation, making the map from $\tilde{\mathbf{X}}$ to Y more difficult to approximate by polynomials (Oladyshkin and Nowak, 2012).

In the applications presented in this paper, we opt for a non-parametric approach to infer the input marginals, and specify f_i by kernel density estimation (KDE) (Rosenblatt, 1956; Parzen, 1962). Given a set $\mathcal{X}_i = \{x_i^{(1)}, \dots, x_i^{(n)}\}$ of observations of X_i , the kernel density estimate \hat{f}_i of f_i reads

$$\hat{f}_i(x) = \frac{1}{nh} \sum_{j=1}^n k\left(\frac{x - x_i^{(j)}}{h}\right), \quad (10)$$

where $k(\cdot)$ is the kernel function and h is the appropriate kernel bandwidth that is learned from the data. Different kernels are used in practice, such as the Epanechnikov or Gaussian kernels. In this paper we use the latter, that is, $k(\cdot)$ is selected as the standard normal PDF.

After estimating the input marginals by KDE, we resort to arbitrary PCE to build a basis of orthonormal polynomials. The PCE metamodel is then trained on $(\mathcal{X}, \mathcal{Y})$.

2.3.3 Truncation schemes

The sum in (6) involves an infinite number of terms. For practical purposes, it is truncated to a finite sum, according to one of various possible truncation schemes. The standard basis truncation (Xiu and Karniadakis, 2002) retains the subset of terms defined by

$$\mathcal{A}^{d,p} = \{\boldsymbol{\alpha} \in \mathbb{N}^d : |\boldsymbol{\alpha}| \leq p\},$$

where $p \in \mathbb{N}^+$ is the chosen maximum polynomial degree and $|\boldsymbol{\alpha}| = \sum_{i=1}^d \alpha_i$ is the total degree of $\Psi_{\boldsymbol{\alpha}}$. Thus, only polynomials of degree up to p are considered. $\mathcal{A}^{d,p}$ contains $\binom{d+p}{p}$ elements. To further reduce the basis size, several additional truncation schemes have been proposed. Hyperbolic truncation (Blatman and Sudret, 2011) retains the polynomials with indices in

$$\mathcal{A}^{d,p,q} = \{\boldsymbol{\alpha} \in \mathcal{A}^{d,p} : \|\boldsymbol{\alpha}\|_q \leq p\},$$

where $q \in (0, 1]$ and $\|\cdot\|_q$ is the q -norm defined by $\|\boldsymbol{\alpha}\|_q = \left(\sum_{i=1}^d \alpha_i^q\right)^{1/q}$.

A complementary strategy is to set a limit to the number of non-zero elements in $\boldsymbol{\alpha}$, that is, to the number of interactions among the components X_i of \mathbf{X} in the expansion. This maximum interaction truncation scheme retains the polynomials with indices in

$$\mathcal{A}^{d,p,r} = \{\boldsymbol{\alpha} \in \mathcal{A}^{d,p} : \|\boldsymbol{\alpha}\|_0 \leq r\},$$

where $\|\boldsymbol{\alpha}\|_0 = \sum_{i=1}^d \mathbf{1}_{\{\alpha_i > 0\}}$.

In our case studies below we combined hyperbolic and maximum truncation, thus retaining the expansion's polynomials with coefficients in

$$\mathcal{A}^{d,p,q,r} = \mathcal{A}^{d,p,q} \cap \mathcal{A}^{d,p,r}, \quad (11)$$

where the triplet (p, q, r) will be selected later on. This choice is motivated by the sparsity of effect principle, which assumes that only few meaningful interactions influence system responses and which holds in most engineering applications.

2.3.4 Calculation of the coefficients

Selected a truncation scheme and the corresponding set $\mathcal{A} = \{\alpha_1, \dots, \alpha_{|\mathcal{A}|}\}$ of multi-indices, the coefficients y_k in

$$Y_{PC}(\mathbf{X}) = \sum_{k=1}^{|\mathcal{A}|} y_k \Psi_{\alpha_k}(\mathbf{X}) \quad (12)$$

need to be determined on the basis of a set $(\mathcal{X}, \mathcal{Y}) = \{(\mathbf{x}^{(j)}, y^{(j)}), j = 1, \dots, n\}$ of observed data. In these settings, the vector $\mathbf{y} = (y_{\alpha_1}, \dots, y_{\alpha_{|\mathcal{A}|}})$ of expansion coefficients can be determined by regression.

When the number $|\mathcal{A}|$ of regressors is smaller than the number n of observations, \mathbf{y} can be determined by solving the ordinary least squares (OLS) problem

$$\mathbf{y} = \arg \min_{\tilde{\mathbf{y}}} \sum_{j=1}^n \left(y^{(j)} - Y_{PC}(\mathbf{x}^{(j)}) \right) = \arg \min_{\tilde{\mathbf{y}}} \sum_{j=1}^n \left(y^{(j)} - \sum_{k=1}^{|\mathcal{A}|} y_k \Psi_{\alpha_k}(\mathbf{x}^{(j)}) \right). \quad (13)$$

The solution reads

$$\mathbf{y} = (\mathbf{A}^T \mathbf{A})^{-1} \mathbf{A}^T \begin{pmatrix} y^{(1)} \\ \vdots \\ y^{(n)} \end{pmatrix}, \quad (14)$$

where $A_{jk} = \Psi_{\alpha_k}(\mathbf{x}^{(j)})$, $j = 1, \dots, n$, $k = 1, \dots, |\mathcal{A}|$.

The OLS problem cannot be solved when $n < |\mathcal{A}|$, because in this case the matrix $\mathbf{A}^T \mathbf{A}$ in (14) is not invertible. Also, OLS tends to overfit the data when $|\mathcal{A}|$ is large. Simpler models with fewer coefficients can be constructed by sparse regression.

Least angle regression (LAR), proposed in Efron et al. (2004), is an algorithm that achieves sparse regression by solving the regularized regression problem

$$\mathbf{y} = \arg \min_{\tilde{\mathbf{y}}} \left\{ \sum_{j=1}^n \left(y^{(j)} - \sum_{k=1}^{|\mathcal{A}|} y_k \Psi_{\alpha_k}(\mathbf{x}^{(j)}) \right) + \lambda \|\tilde{\mathbf{y}}\|_1 \right\}. \quad (15)$$

The last addendum in the expression is the regularization term, which forces the minimisation to favour sparse solutions. The use of LAR in the context of PCE was initially proposed in Blatman and Sudret (2011), which the reader is referred to for more details. In the applications illustrated in Sections 3 and 4, we adopt LAR to determine the PCE coefficients.

2.3.5 Estimation of the output statistics

Given the statistical model $F_{\mathbf{Z}}$ of the input and the PCE metamodel (12) of the input-output map, the model response Y_{PC} is not only known pointwise, but can also be characterized statistically. For instance, the orthonormality of the polynomial basis ensures that the mean and the variance of Y_{PC} read, respectively,

$$\mathbb{E}[Y_{\text{PC}}] = y_0, \quad \mathbb{V}[Y_{\text{PC}}] = \sum_{\alpha \in \mathcal{A} \setminus \{\mathbf{0}\}} y_{\alpha}^2. \quad (16)$$

This property provides a useful interpretation of the expansion coefficients in terms of the first two moments of the output. Other output statistics, such as the Sobol partial sensitivity indices (Sobol', 1993), can be obtained from the expansion coefficients analytically (Sudret, 2008).

Higher-order moments of the output, as well as other statistics (such as the full PDF F_Y), can be efficiently estimated through Monte-Carlo simulation, by sampling sufficiently many realisations of \mathbf{X} and evaluating the corresponding PCE responses. Polynomial evaluation is computationally cheap and can be trivially vectorized, making estimation by resampling extremely efficient.

2.4 PCE for mutually dependent inputs

If the input vector \mathbf{X} has statistically dependent components, its joint PDF $f_{\mathbf{X}}$ is not the product of the marginals and the orthogonality property (5) does not hold. As a consequence, one cannot construct multivariate orthogonal polynomials by tensor product of univariate ones, as done in (7). Constructing a basis of orthogonal polynomials in this general case is still possible, but computationally demanding. For this reason, we investigate two alternative strategies.

The first strategy consists in ignoring the input dependencies and in building a basis of polynomials orthonormal with respect to $\prod_i f_i(x_i)$ by arbitrary PCE. This approach is labelled from here on as *aPCEonX*. While not forming a basis of the space of square integrable functions with respect to $f_{\mathbf{X}}$, the considered set of polynomials may still yield a similarly good pointwise approximation.

Accurate estimates of the output statistics may be obtained *a posteriori* by modelling the input dependencies through copula functions, as detailed in Appendix A. The joint CDF of a random vector \mathbf{X} with copula distribution $C_{\mathbf{X}}$ and marginals F_i (here, obtained by KDE) is given by (A.1). Resampling from such a probabilistic input model yields more accurate estimates of the output statistics than resampling from the distribution $\prod_i F_i(x_i)$, that is, than ignoring dependencies.

The second possible approach, presented in more details in Appendix B, consists in modelling directly the input dependencies by copulas, and then in transforming the input vector \mathbf{X} into a set of independent random variables \mathbf{Z} with prescribed marginals (*e.g.*,

standard uniform) through the associated Rosenblatt transform $\mathcal{T}^{(\Pi)}$ (Rosenblatt, 1952), defined in (A.18). The PCE metamodel is then built between the transformed input vector \mathbf{Z} and the output Y . When the input marginals are standard uniform distributions, the corresponding class of orthonormal polynomials is the Legendre family, and the resulting PCE is here indicated by *lPCEonZ*. The asymptotic properties of an orthonormal PCE, such as the relations (16), hold. The expression of Y in terms of \mathbf{X} is given by the relation (B.1).

At first, the second approach seems advantageous over the first one. It involves, in a different order, the same steps: modelling the input marginals and copula, and building the PCE metamodel. By capturing dependencies earlier on, it enables the construction of a basis of mutually orthonormal polynomials with respect to the joint PDF of the (transformed) inputs. It thereby provides a model with spectral properties (except for unavoidable errors due to truncation and parameter fitting). The experiments run in Section 3, however, show that the first approach yields typically more accurate pointwise predictions (although not necessarily better statistical estimates). This is due to the fact that it avoids mapping the input \mathbf{X} into independent variables \mathbf{Z} via the (typically strongly non-linear) Rosenblatt transform. For a more detailed discussion, see Section 3.4.

3 Validation on synthetic data

3.1 Validation scheme

We first investigate data-driven regression by PCE on two different simulated data sets. The first data set is obtained through an analytical, highly non-linear function of three variables, subject to three uncertain inputs. The second data set is a finite element model of a horizontal truss structure, subject to 10 uncertain inputs. In both cases, the inputs are statistically dependent, and their dependence is modelled through a canonical vine (C-vine) copula (see Appendix A).

We study the performance of the two alternative approaches described in Section 2.4: *aPCEonX* and *lPCEonZ*. In both cases we model the input copula as a C-vine, fully inferred from the data. For the *aPCEonX* the choice of the copula only plays a role in the estimation of the output statistics, while for the *lPCEonZ* it affects also the pointwise predictions. We additionally tested the performance obtained by using the true input copula (known here because it was used to generate the synthetic data) and a Gaussian copula inferred from data. We also investigated the performance obtained by using the true marginals instead of the ones fitted by KDE. Using the true copula and marginals yielded better statistical estimates, but is of little practical interest, as it would not be known in real applications. The Gaussian copula yielded generally similar or slightly worse accuracy. For brevity, we do not show these results.

To assess the pointwise accuracy, we generate a training set $(\mathcal{X}', \mathcal{Y}')$ of increasing size n' ,

build the PCE metamodels both by *aPCEonX* and by *lPCEonZ*, and evaluate their rMAE on a validation set $(\mathcal{X}'', \mathcal{Y}'')$ of fixed size $n'' = 10,000$ points. The statistical accuracy is quantified instead in terms of error on the mean, standard deviation, and full PDF of the true models by (2)-(4). The statistical estimates obtained by the two PCE approaches are furthermore compared to the corresponding sample estimates obtained from the same training data (sample mean, sample standard deviation, and KDE of the PDF)

For each value of n' and each error type, error bands are obtained as the minimum to maximum error obtained across 10 different realisations of $(\mathcal{X}', \mathcal{Y}')$ and $(\mathcal{X}'', \mathcal{Y}'')$. The minimum error is often taken in machine learning studies as an indication of the best performance that can be delivered by a given algorithm in a given task. The maximum error represent analogously the worst-case scenario.

Finally, we assess the robustness to noise by adding a random perturbation ε to each output observations in \mathcal{Y}' used to train the PCE model. The noise is drawn independently for each observation from a univariate Gaussian distribution with mean $\mu_\varepsilon = 0$ and prescribed standard deviation σ_ε .

3.2 Ishigami function

The first model we consider is

$$Y = 1 + \frac{\text{ish}(X_1, X_2, X_3) + 1 + \pi^4/10}{9 + \pi^4/5}, \quad (17)$$

where

$$\text{ish}(x_1, x_2, x_3) = \sin(x_1) + 7 \sin^2(x_2) + 0.1x_3^4 \sin(x_1) \quad (18)$$

is the Ishigami function (Ishigami and Homma, 1990), defined for inputs $x_i \in [-\pi, \pi]$ and taking values in $[-1 - \frac{\pi^4}{10}, 8 + \frac{\pi^4}{10}]$. The Ishigami function is often used as a test case in global sensitivity analysis due to its strong non-linearity and non-monotonicity. Model (17) is rescaled here to take values in the interval $[1, 2]$. Rescaling does not affect the approximation accuracy of the PCE, but enables a meaningful evaluation of the rMAE (2) by avoiding values of Y close to 0.

We model the input \mathbf{X} as a random vector with marginals $X_i \sim \mathcal{U}([-\pi, \pi])$, $i = 1, 2, 3$, and C-vine copula with density

$$c_{\mathbf{X}}(u_1, u_2, u_3) = c_{12}^{(\mathcal{G})}(u_1, u_2; 2) \cdot c_{13}^{(t)}(u_1, u_3; 0.5, 3).$$

Here, $c_{12}^{(\mathcal{G})}(\cdot, \cdot; \theta)$ and $c_{13}^{(t)}(\cdot, \cdot; \theta)$ are the densities of the pairwise Gumbel and t- copula families defined in rows 11 and 19 of Table A.4. Thus, X_1 correlates positively with both X_2 and X_3 . X_2 and X_3 are also positively correlated, but conditionally independent given X_1 . The joint CDF of \mathbf{X} can be obtained from its marginals and copula through (A.1). The PDF of Y in response to input \mathbf{X} , its mean μ_Y and its standard deviation σ_Y , obtained on 10^7 sample points, are shown in the left panel of Figure 1.

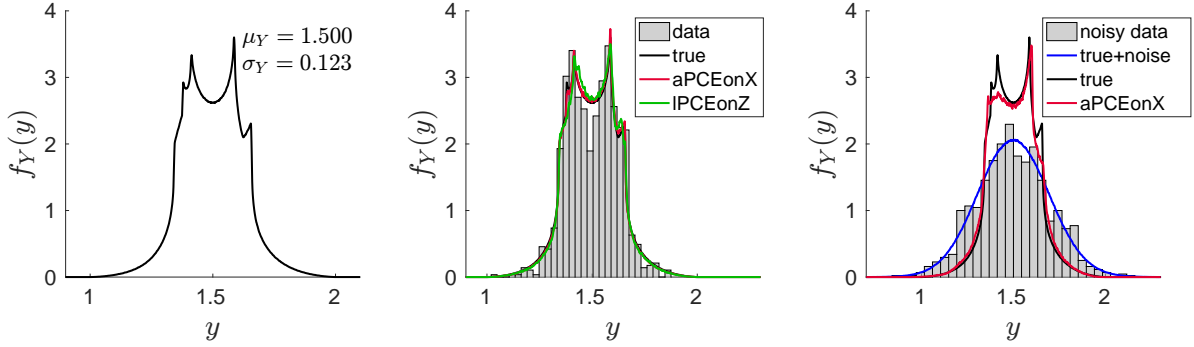


Figure 1: **Response PDFs of the Ishigami function.** *Left panel:* true PDF f_Y of the Ishigami model's response, obtained on 10^7 sample points by KDE. *Central panel:* histogram obtained from $n' = 1,000$ output observations used for training (gray bars), true response PDF as in the left panel (black), PDFs obtained from the $aPCEonX$ (red) and the $lPCEonZ$ (green) by resampling. *Right panel:* as in the central panel, but for training data perturbed with Gaussian noise ($\sigma_\varepsilon = 0.15 = 1.22 \sigma_Y$). The blue line indicates the true PDF of the perturbed model.

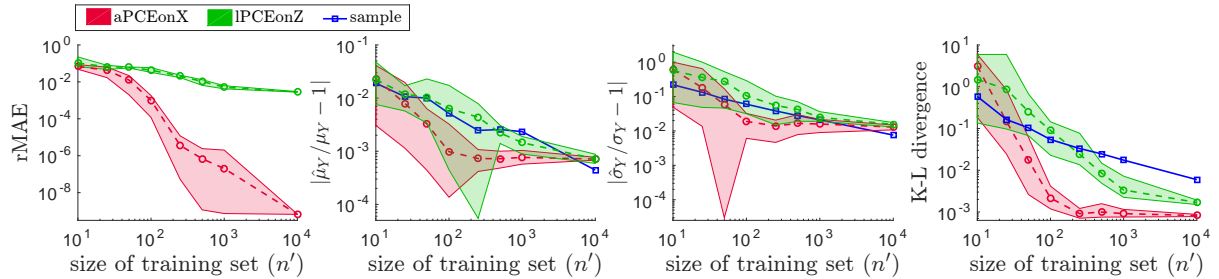


Figure 2: **PCE of Ishigami model: performance.** From left to right: rMAE, error on the mean, error on the standard deviation, and Kullback-Leibler divergence of $aPCEonX$ (red) and $lPCEonZ$ (green), for a size n' of the training set increasing from 10 to 10,000. The dash-dotted lines and the bands indicate, respectively, the average and the minimum to maximum errors over 10 simulations. In the second to fourth panels, the blue lines correspond to the empirical estimates obtained from the training data (error bands not shown).

Next, we build the $aPCEonX$ and the $lPCEonZ$ on training data $(\mathcal{X}', \mathcal{Y}')$, and assess their performance as described in Section 3.1. The errors are shown in Figure 2 (red: $aPCEonX$; green: $lPCEonZ$), as a function of the training set size n' . The dotted line indicates the average error over the 10 repetitions, while the shaded area around it spans the range from the minimum to the maximum error across 10 repetitions. The $aPCEonX$ yields a considerably lower rMAE. This is due to the strong non-linearity of the Rosenblatt transform used by the $lPCEonZ$ to de-couple the components of the input data. Importantly, the methodology works well already in the presence of relatively few data points: the pointwise error and the Kullback-Leibler divergence both drop below 1% when using as few as $n' = 100$ data points. The central panel of Figure 1 shows the histogram obtained from $n' = 1,000$ output observations of one training set, the true PDF (black), and the PDFs obtained by resampling from the $aPCEonX$ and the $lPCEonZ$ built on that training set. The statistics

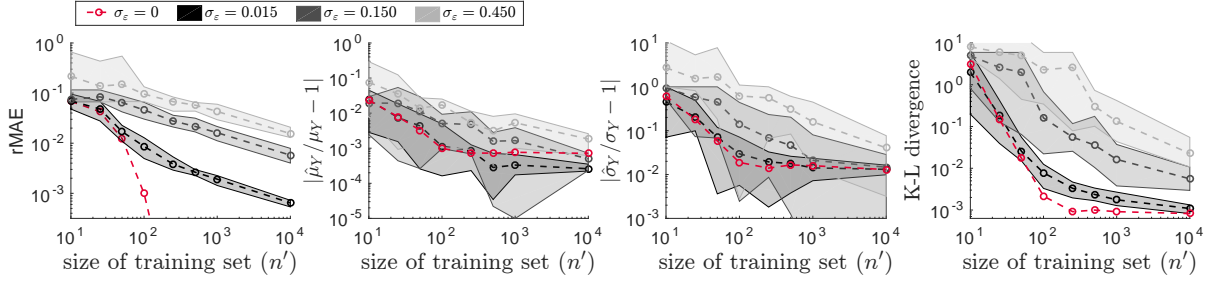


Figure 3: ***aPCEonX* of Ishigami model: robustness to noise (for multiple noise levels).** From left to right: rMAE, error on the mean, error on the standard deviation, and Kullback-Leibler divergence of the *aPCEonX* for an increasing amount of noise: $\sigma_\varepsilon = 0.015$ (dark gray), $\sigma_\varepsilon = 0.15$ (mid-light gray), and $\sigma_\varepsilon = 0.45$ (light gray). The dash-dotted lines and the bands indicate, respectively, the average and the minimum to maximum error over 10 simulations. The red lines, reported from Figure 2 for reference, indicate the mean error obtained for the noise-free data.

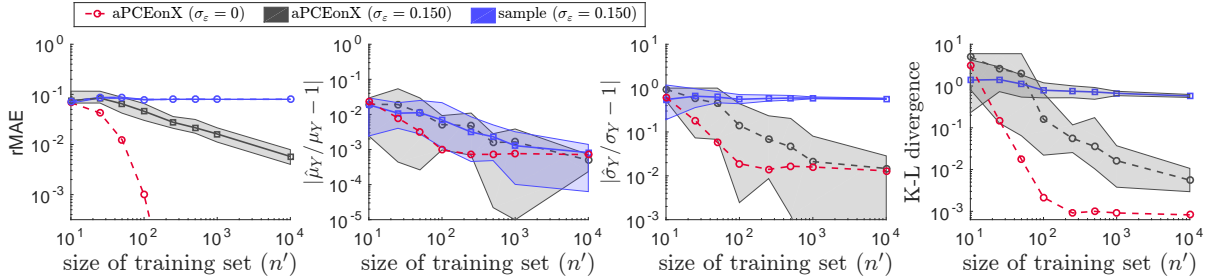


Figure 4: ***aPCEonX* of Ishigami model: robustness to noise (w.r.t. sample estimation).** From left to right: rMAE, error on the mean, error on the standard deviation, and Kullback-Leibler divergence obtained by *aPCEonX* (gray) and by direct sample estimation (blue), for noise $\sigma_\varepsilon = 0.15 = 1.22\sigma_Y$. The dash-dotted lines and the bands indicate, respectively, the average and the minimum to maximum error over 10 simulations. The red lines, reported from Figure 2 for reference, indicate the mean error obtained for the noise-free data.

of the true response are better approximated by the *aPCEonX* than by the *lPCEonZ* or by sample estimation (blue solid lines in Figure 2).

Finally, we examine the robustness of *aPCEonX* to noise. We perturb each observation in \mathcal{Y} by adding noise drawn from a Gaussian distribution with mean 0 and standard deviation σ_ε . σ_ε is assigned as a fixed proportion of the model's true mean μ_Y : 1%, 10%, and 30% of μ_Y (corresponding to 12%, 122%, and 367% of σ_Y , respectively). The results, shown in Figures 3-4, indicate that the methodology is robust to noise. Indeed, the errors of all types are significantly smaller than the magnitude of the added noise, and decrease with increasing sample size (see Figure 3). For instance, the rMAE for $\sigma_\varepsilon = 0.15 = 1.22\sigma_Y$ drops to 10^{-2} if 100 or more training points are used. The error on μ_Y is minorly affected, which is expected since the noise is unbiased. More importantly, σ_Y and f_Y can be recovered with high precision even in the presence of strong noise (see also Figure 1, fourth panel). In this case, the PCE predictor for the standard deviation works significantly better than the sample

estimates, as illustrated in Figure 4.

3.3 23-bar horizontal truss

We further replicate the analysis carried out in the previous section on a more complex finite element model of a horizontal truss (Blatman and Sudret, 2011). The structure consists of 23 bars connected at 6 upper nodes, and is 24 meters long and 2 meters high (see Figure 5). The bars belong to two different groups (horizontal and diagonal bars), both having uncertain Young modulus E_i and uncertain cross-sectional area A_i , $i = 1, 2$:

$$\begin{aligned} E_1, E_2 &\sim \mathcal{LN}(2.1 \cdot 10^{11}, 2.1 \cdot 10^{10}) \text{ Pa}, \\ A_1 &\sim \mathcal{LN}(2.0 \cdot 10^{-3}, 2.0 \cdot 10^{-4}) \text{ m}^2, \\ A_2 &\sim \mathcal{LN}(1.0 \cdot 10^{-3}, 1.0 \cdot 10^{-4}) \text{ m}^2, \end{aligned}$$

where $\mathcal{LN}(\mu, \sigma)$ is the univariate lognormal distribution with mean μ and standard deviation σ .

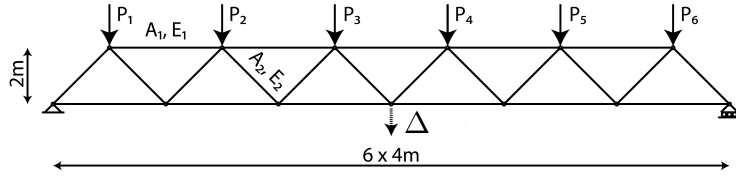


Figure 5: **Scheme of the horizontal truss model.** 23-bar horizontal truss with bar cross-section A_i and Young modulus E_i ($i = 1, 2$: horizontal and vertical bars, respectively), subject to loads P_1, \dots, P_6 . Modified from Blatman and Sudret (2011).

The four variables can be considered statistically independent, and their values influence the structural response to loading. An additional source of uncertainty comes from six random loads P_1, P_2, \dots, P_6 the truss is subject to, one on each upper node. The loads have Gumbel marginal distribution with mean $\mu = 5 \times 10^4$ N and standard deviation $\sigma = 0.15\mu = 7.5 \times 10^3$ N:

$$F_i(x; \alpha, \beta) = e^{-e^{-(x-\alpha)/\beta}}, \quad x \in \mathbb{R}, i = 1, 2, \dots, 6, \quad (19)$$

where $\beta = \sqrt{6}\sigma/\pi$, $\alpha = \mu - \gamma\beta$, and $\gamma \approx 0.5772$ is the Euler-Mascheroni constant. In addition, the loads are made mutually dependent through the C-vine copula with density

$$c_{\mathbf{X}}^{(\mathcal{G})}(u_1, \dots, u_6) = \prod_{j=2}^6 c_{1j; \theta=1.1}^{(\mathcal{GH})}(u_1, u_j), \quad (20)$$

where each $c_{1j; \theta}^{(\mathcal{GH})}$ is the density of the pair-copula between P_1 and P_j , $j = 2, \dots, d$, and belongs to the Gumbel-Hougaard family defined in Table A.4, row 11.

The presence of the loads causes a downward vertical displacement Δ at the mid span of the structure. Δ is taken to be the system's uncertain response to the 10-dimensional

random input $\mathbf{X} = (E_1, E_2, A_1, A_2, P_1, \dots, P_6)$ consisting of the 4 structural variables and the 6 loads. The true statistics (mean, standard deviation, PDF) of Δ are obtained by MCS over 10^7 sample points, and are shown in the left panel of Figure 6.

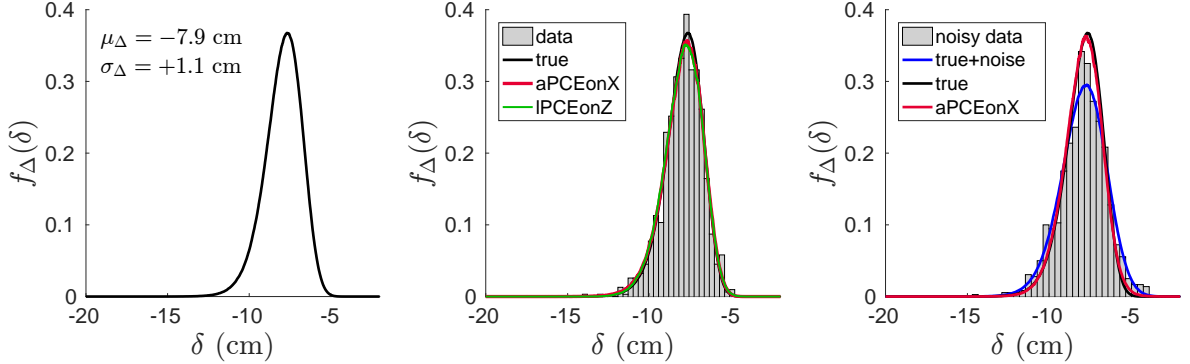


Figure 6: **Response PDFs of the horizontal truss.** *Left panel:* true PDF f_Y of the truss response, obtained on 10^7 sample points by KDE. *Central panel:* probability histogram obtained from $n' = 1,000$ output observations used for training (gray bars), true response PDF as in the left panel (black), PDFs obtained from the *aPCEonX* (red) and the *lPCEonZ* (green) by resampling. *Right panel:* as in the central panel, but for training data perturbed with Gaussian noise ($\sigma_\varepsilon = 0.79 \text{ cm} = 0.70\sigma_\Delta$). The blue line indicates the true PDF of the perturbed model.

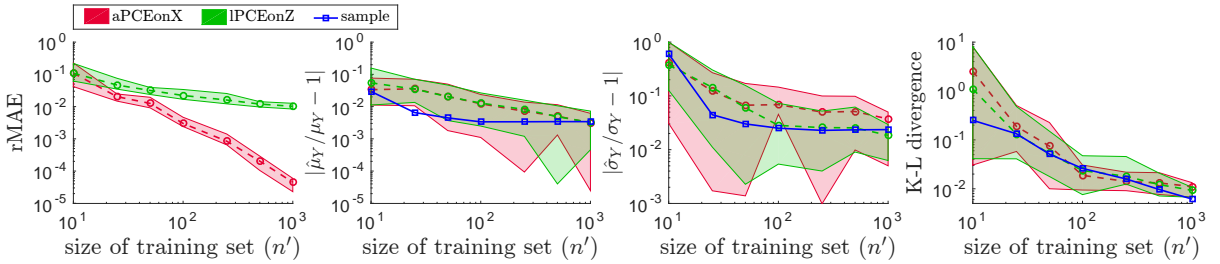


Figure 7: **PCE performance for the horizontal truss.** From left to right: rMAE, error on the mean, error on the standard deviation, and Kullback-Leibler divergence of *aPCEonX* (red) and *lPCEonZ* (green), for a size n' of the training set increasing from 10 to 1,000. The dash-dotted lines and the bands indicate, respectively, the average and the minimum to maximum errors over 10 simulations. In the second to fourth panels, the blue lines correspond to the empirical estimates obtained from the training data (error bands not shown).

We analyse the system with the same procedure undertaken for the Ishigami model: we build *aPCEonX* and *lPCEonZ* on each of 10 training sets $(\mathcal{X}', \mathcal{Y}')$ of increasing size n' , and validate their performance. The pointwise error is evaluated on 10 validation sets $(\mathcal{X}'', \mathcal{Y}'')$ of fixed size $n'' = 10,000$, while the statistical errors are determined by large resampling.

The results are shown in Figure 7. Both PCEs exhibit high performance, yet the *aPCEonX* yields a significantly smaller pointwise error (first panel). The *lPCEonZ* yields a better estimate of the standard deviation, yet the empirical estimates obtained from the training data are the most accurate ones in this case.

Having selected the *aPCEonX* as the better of the two metamodels, we further assess

its performance in the presence of noise. We perturb the response values used to train the model by adding Gaussian noise with increasing standard deviation σ_ε , set to 1%, 10%, and 30% of $|\mu_\Delta|$ (equivalent to 7%, 70%, and 210% of σ_Δ , respectively). The results are shown in Figures 8-9. The errors of all types are significantly smaller than the magnitude of the added noise, and decrease with increasing sample size for all noise levels (Figure 8). Also, the PCE estimates are significantly better than the sample estimates (Figure 9; see also Figure 6, fourth panel).

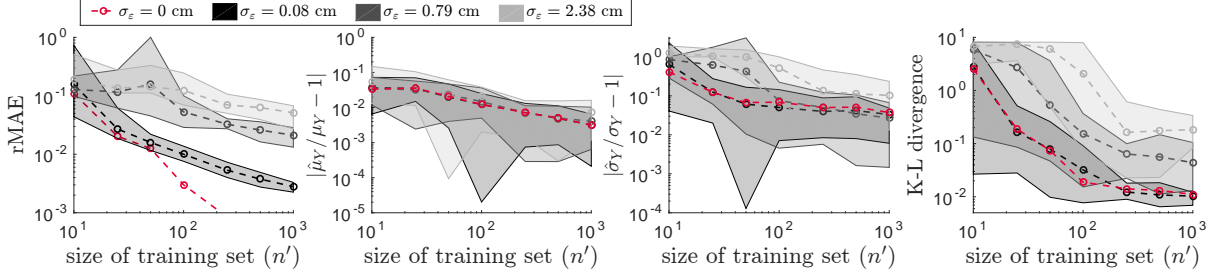


Figure 8: ***aPCEonX* of horizontal truss: robustness to noise (for multiple noise levels)**. From left to right: rMAE, error on the mean, error on the standard deviation, and Kullback-Leibler divergence of *aPCEonX* for an increasing amount of noise: $\sigma_\varepsilon = 0.079$ cm (dark gray), $\sigma_\varepsilon = 0.79$ cm (mid-light gray), and $\sigma_\varepsilon = 2.38$ cm (light gray). The dash-dotted lines and the bands indicate, respectively, the average and the minimum to maximum error over 10 simulations. The red lines, reported from Figure 7 for reference, indicate the error for the noise-free data.

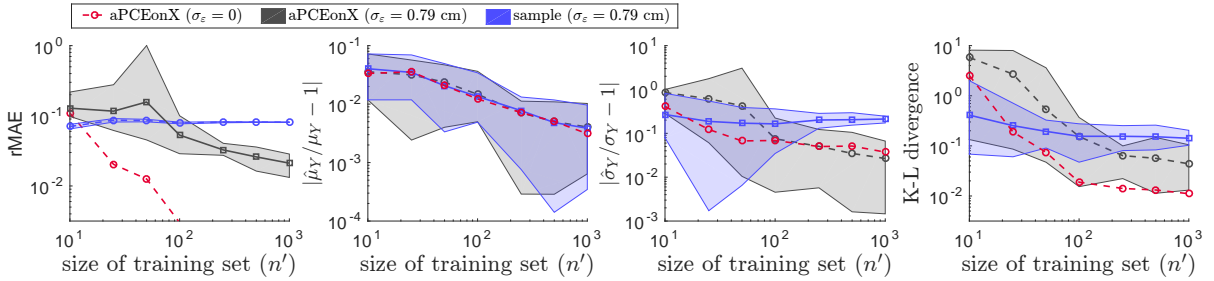


Figure 9: ***aPCEonX* of horizontal truss: robustness to noise (w.r.t. sample estimation)**. From left to right: rMAE, error on the mean, error on the standard deviation, and Kullback-Leibler divergence obtained by *aPCEonX* (gray) and by direct sample estimation (blue), for noise $\sigma_\varepsilon = 0.79$ cm = $0.7 \sigma_Y$. The dash-dotted lines and the bands indicate, respectively, the average and the minimum to maximum error over 10 simulations. The red lines, reported from Figure 2 for reference, indicate the mean error obtained for the noise-free data.

3.4 Preliminary conclusion

The results obtained in the previous section allow us to draw some important preliminary conclusions on data-driven PCE. The methodology:

- delivers reliable predictions of the system response to multivariate inputs;

- produces reliable estimates of the response statistics if the input dependencies are properly modelled, as done here through copulas (for *aPCEonX*: a-posteriori);
- works well already when trained on few observations;
- deals effectively with noise, thus providing a tool for denoising;
- involves only few hyperparameters: the range of degrees allowed for the PCE and the truncation parameters. All have a clear meaning and require little tuning.

In order to build the expansion when the inputs are mutually dependent, we investigated two alternative approaches, labelled as *lPCEonZ* and *aPCEonX*. Of the two strategies, *aPCEonX* appears to be the most effective one in purely data-driven problems. It is worth mentioning, though, that *lPCEonZ* may provide superior statistical estimates if the joint distribution of the input is known with greater accuracy than in the examples shown here. This was the case, for instance, when we replaced the inferred marginals and copula used to build the *lPCEonZ* with the true ones (not shown here): in both examples above, we obtained more accurate estimates of μ_Y , σ_Y , and F_Y (but not better pointwise predictions) than using *aPCEonX*.

4 Results on real data sets

We now demonstrate the use of *aPCEonX* on three different real data sets. The selected data sets were previously analysed by other authors with different machine learning algorithms, which establish here the performance benchmark.

4.1 Analysis workflow

4.1.1 Statistical input model

The considered data sets comprise samples made of multiple input quantities and one scalar output. Adopting the methodology outlined in Section 2, we characterize the multivariate input \mathbf{X} statistically by modelling its marginals \hat{f}_i through KDE, and we then resort to arbitrary PCE to express the output Y as a polynomial of \mathbf{X} . The basis of the expansion thus consists of mutually orthonormal polynomials with respect to $\prod_i \hat{f}_i(x_i)$, where \hat{f}_i is the marginal PDF inferred for X_i .

4.1.2 Estimation of pointwise accuracy

Following the pointwise error assessment procedure carried out in the original publications, for the case studies considered here we assess the method’s performance by cross-validation. Standard k -fold cross-validation partitions the data $(\mathcal{X}, \mathcal{Y})$ into k subsets, trains the model on $k - 1$ of those (the training set $(\mathcal{X}', \mathcal{Y}')$), and assesses the pointwise error between the model’s predictions and the observations on the k -th one (the validation set $(\mathcal{X}'', \mathcal{Y}'')$). The

procedure is then iterated over all k possible combinations of training and validation sets. The final error is computed as the average error over all validation sets. The number k of data subsets is chosen as in the reference studies. Differently from the synthetic models considered in the previous section, the true statistics of the system response are not known here, and the error on their estimates cannot be assessed.

A variation on standard cross-validation consists in performing a k -fold cross validation on each of multiple random shuffles of the data. The error is then typically reported as the average error obtained across all randomisations, ensuring that the final results are robust to the specific partitioning of the data in its k subsets. In the following, we refer to a k -fold cross validation performed on r random permutations of the data (i.e. r random k -fold partitions) as an $r \times k$ -fold randomised cross-validation.

4.1.3 Statistical estimation

Finally, we estimate for all cases studies the response PDF a-posteriori (AP) by resampling. To this end, we first model their dependencies through a C-vine copula $\hat{C}^{(\nu)}$. The vine is inferred from the data as detailed in Appendix A.3. Afterwards, resampling involves the following steps:

- sample n_{AP} points $\mathcal{Z}_{\text{AP}} = \{\mathbf{z}^{(l)}, l = 1, \dots, n_{\text{AP}}\}$ from $\mathbf{Z} \sim U([0, 1]^d)$. We opt for Sobol' quasi-random low-discrepancy sequences (Sobol', 1967), and set $n_{\text{AP}} = 10^6$;
- map $\mathcal{Z}_{\text{AP}} \mapsto \mathbf{U}_{\text{AP}} \subset [0, 1]^d$ by the inverse Rosenblatt transform of $\hat{C}^{(\nu)}$;
- map $\mathbf{U}_{\text{AP}} \mapsto \mathcal{X}_{\text{AP}}$ by the inverse probability integral transform of each marginal CDF \hat{F}_i . \mathcal{X}_{AP} is a sample set of input observations with copula $\hat{C}^{(\nu)}$ and marginals \hat{F}_i ;
- evaluate the set $\mathcal{Y}_{\text{AP}} = \{y_{\text{PC}}^{(l)} = \mathcal{M}_{\text{PC}}(\mathbf{x}), \mathbf{x} \in \mathcal{X}_{\text{AP}}\}$ of responses to the inputs in \mathcal{X}_{AP} .

The PDF of Y is estimated on \mathcal{Y}_{AP} by kernel density estimation.

4.2 Combined-cycle power plant

The first real data set we consider consists of 9,568 data points collected from a combined-cycle power plant (CCPP) over 6 years (2006-2011). The CCPP generates electricity by gas and steam turbines, combined in one cycle. The data comprise 4 ambient variables and the energy production E , measured over time. The four ambient variables are the temperature T , the pressure P and the relative humidity H measured in the gas turbine, and the exhaust vacuum V measured in the steam turbine. All five quantities are hourly averages. The data are available online (Lichman, 2013).

The data were analysed in Tüfekci (2014) with neural network- (NN-) based ML methods to predict the energy output based on the measured ambient variables. The authors assessed the performance of various learners by 5×2 -fold randomised cross-validation, yielding a total of 10 pairs of training and validation sets. Each set contained 4,784 observations. The best

	MAE	min. MAE	mean-min	rMAE (%)
<i>aPCEonX</i>	3.11 ± 0.03	3.05	0.06	0.68 ± 0.007
BREP-NN (Tüfekci, 2014)	$3.22 \pm \text{n.a.}$	2.82	0.40	n.a.

Table 1: **Errors on CCPP data.** MAE yielded by the *aPCEonX* (first row) and by the BREP-NN model in Tüfekci (2014) (second row). From left to right: average MAE \pm its standard deviation over all 10 validation sets (in MWh), its minimum (error on the “best set”), difference between the average and the minimum MAEs, and rMAE.

learner among those tested by the authors was a bagging reduced error pruning (BREP) NN, which yielded a mean MAE of 3.22 MWh (see their Table 10, row 4). The lowest MAE of this model over the 10 validation sets, corresponding to the “best” validation set, was indicated to be 2.82 MWh. Besides providing an indicative lower bound to the errors, the minimum gives, when compared to the means, an indication of the variability of the performance over different partitions of the data. The actual error variance over the 10 validation sets was not provided in the mentioned study.

We analyze the very same 10 training sets by PCE. The results are reported in Table 1. The average MAE yielded by the *aPCEonX* is slightly smaller than that of the BREP NN model. More importantly, the difference between the average and the minimum error, calculated over the 10 validation sets, is significantly lower with our approach, indicating a lower sensitivity of the results to the partition of the data, and therefore a higher reliability in the presence of random observations. The average error of the PCE predictions relative to the observed values is below 1%.

Finally, we estimate the PDF of the hourly energy produced by the CCPP following the procedure described in Section 4.1.3. The results are shown in Figure 10. Reliable estimates of the energy PDF aid for instance energy production planning and management.

4.3 Boston Housing

The second real data set used to validate the PCE-based ML method concerns housing values in the suburbs of Boston, collected in 1970. The data set, downloaded from Lichman (2013), was first published in Harrison and Rubinfeld (1978), and is a known reference in the machine learning and data mining communities.

The data comprise 506 instances, each having 14 attributes. One attribute (the proximity of the neighborhood to the Charles river) is binary-valued and is therefore disregarded in our analysis. Of the remaining 13 attributes, one is the median housing value of owner-occupied homes in the neighbourhood, in thousands of \$ (MEDV). The remaining 12 attributes are, in order: the per capita crime rate by town (CRIM), the proportion of residential land zones for lots over 25,000 sq.ft. (ZN), the proportion of non-retail business acres per town (INDUS),

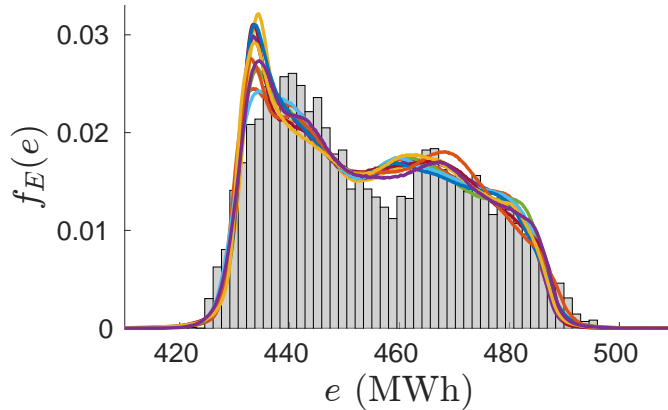


Figure 10: **Estimated PDF of the energy produced by the CCPP.** The bars indicate the histogram obtained from the observed CCPP energy output. The coloured lines show the PDFs of the PCE metamodells built on the 10 training sets, for input dependencies modelled by C-vines.

the nitric oxides concentration, in parts per 10 million (NOX), the average number of rooms per dwelling (RM), the proportion of owner-occupied units built prior to 1940 (AGE), the weighted distances to five Boston employment centres (DIS), the index of accessibility to radial highways (RAD), the full-value property-tax rate per \$10,000 (TAX), the pupil-teacher ratio by town (PTRATIO), the index $1,000(\text{Bk} - 0.63)^2$, where Bk is the proportion of black residents by town, and the lower status of the population (LSTAT).

The data were analysed in previous studies with different regression methods to predict the median house values MEDV on the basis of the other attributes (Can, 1992; Gilley and Pace, 1995; Quinlan, 1993; R Kelley Pace, 1997). The original publication itself (Harrison and Rubinfeld, 1978) was concerned with determining whether the demand for clean air affected housing prices. The data were analysed with different supervised learning methods in Quinlan (1993). Among them, the best predictor was shown to be an NN model combined with instance-based learning, yielding $\text{MAE} = 2,230\$$ (rMAE: 12.9%) on a 10-fold cross-validation.

We model the data by PCE and quantify the performance by 10×10 randomised cross-validation. The results are summarized in Table 2. The errors are comparable to the NN model with instance based learning in Quinlan (1993). While the latter yields the lowest absolute error, the *aPCEonX* achieves a smaller relative error. In addition, it does not require the fine parameter tuning that affects most NN models. Finally, we estimate the PDF of the median house value as described in Section 4.1.3. The results are shown in Figure 11.

	MAE (\$)	rMAE (%)
<i>aPCEonX</i>	2483 ± 337	12.6 ± 2.0
NN (Quinlan, 1993)	$2230 \pm \text{n.a.}$	$12.9 \pm \text{n.a.}$

Table 2: **Errors on Boston Housing data.** MAE and rMAE yielded by the *aPCEonX* (first row) and by the NN model with instance based learning from Quinlan (1993) (second row).

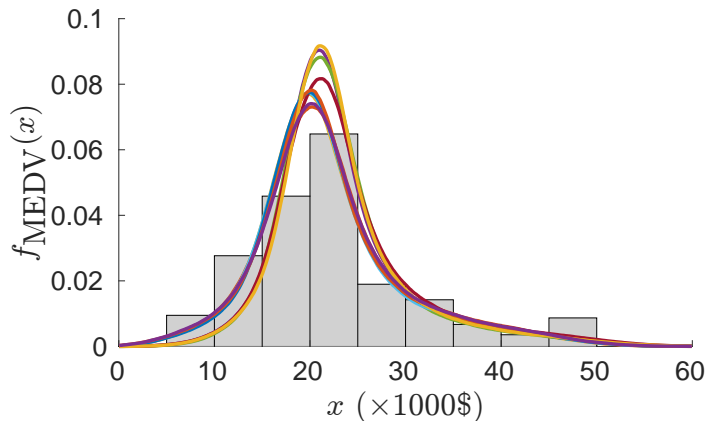


Figure 11: **Estimated PDF of the variable MEDV.** The bars indicate the sample PDF, as an histogram obtained using 50 bins from \$0 to \$50k (the maximum house value in the data set). The coloured lines show the PDFs of the PCE metamodells built on 10 of the 100 training sets (one per randomization of the data), for input dependencies modelled by C-vines. The dots indicate the integrals of the estimated PDFs for house values above \$49k.

4.4 Wine quality

The third real data set we consider concerns the quality of wines from the *vinho verde* region in Portugal. The data set consists of 1,599 red samples and 4,898 white samples, collected between 2004 and 2007. The data are available online at <http://www3.dsi.uminho.pt/pcortez/wine/>. Each wine sample was analysed in laboratory for 11 physico-chemical parameters: fixed acidity, volatile acidity, citric acid, residual sugar, chlorides, free sulfur dioxide, total sulfur dioxide, density, pH, sulphates, alcohol. In addition, each sample was given a quality score Q based on blinded sensory tests from three or more sensory assessors. The score is the median of the grades (integers between 0 and 10) assigned by each assessor.

The data were previously analysed in Cortez et al. (2009) to predict the wine quality score on the basis of the 11 physico-chemical parameters. The study compared various ML algorithms, namely multiple regression, different types of NN, and support vector machine (SVM, see Schölkopf and Smola (2002)) regression. SVM regression outperformed the other methods, yielding the lowest MAE, as assessed by means of 20×5 -fold randomised cross-validation.

We model the data by $aPCEonX$, and round the predicted wine ratings, which take continuous predicted values, to their closest integer. The performance is then assessed through the same cross-validation procedure used in Cortez et al. (2009). The results are reported in Table 3. The MAE of $aPCEonX$ is comparable to that of the SVM regressor, and always lower than the best NN.

	red wine:		white wine:	
	MAE	rMAE (%)	MAE	rMAE (%)
$aPCEonX$	0.44 ± 0.03	8.0 ± 0.6	0.50 ± 0.02	8.8 ± 0.3
SVM in Cortez et al. (2009)	0.46 ± 0.00	n.a.	0.45 ± 0.00	n.a.
Best NN in Cortez et al. (2009)	0.51 ± 0.00	n.a.	0.58 ± 0.00	n.a.

Table 3: **Errors on wine data.** MAE and rMAE yielded on red and white wine data by the $aPCEonX$, by the SVM in Cortez et al. (2009), and by the best NN model in Cortez et al. (2009).

Finally, our framework enables the estimation of the PDF of the wine rating as predicted by the PCE metamodells. The resulting PDFs are shown in Figure 12. One could analogously compute the conditional PDFs given by fixing any subset of inputs to given values (*e.g.*, the residual sugar or alcohol content, which can be easily controlled in the wine making process). This may help, for instance, predicting the wine quality for fixed physico-chemical parameters, or choosing the latter so as to optimize the wine quality or to minimize its uncertainty. This analysis goes beyond the scope of the present work.

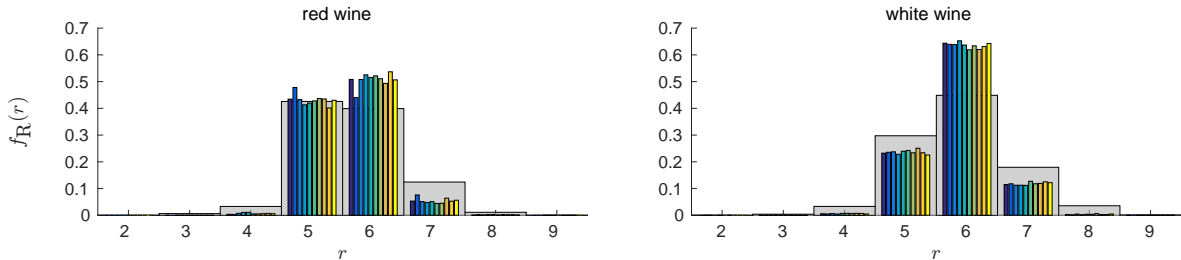


Figure 12: **Estimated PDF of the wine rating.** For each panel (left: red wine; right: white wine), the grey bars indicate the sample PDF of the median wine quality score assigned by the assessors. The coloured bars show the predicted PDFs obtained by resampling from the PCE metamodells built on 10 of the 100 total training sets, for input dependencies modelled by C-vines.

5 Discussion and conclusions

We proposed an approach to machine learning (ML) that capitalises on polynomial chaos expansion (PCE), an advanced regression technique from uncertainty quantification. PCE is a popular spectral method in engineering applications, where it is often used to replace expensive-to-run computational models subject to uncertain inputs with an inexpensive metamodel that retains the statistics of the output (*e.g.*, moments, PDF). Our paper shows that PCE can also be used as an effective regression model in purely data driven problems, where only input observations and corresponding system responses - but no computational model of the system - are available.

We tested the performance of PCE on simulated data first, and then on real data by cross-validation. The reference performance measure was the average point-wise error of the PCE metamodel over all test data. The simulations also allowed us to assess the ability of PCE to estimate the statistics of the response (its mean, standard deviation, and PDF) in the considered data-driven scenario. Both the point-wise and the statistical errors of the methodology were low, even when relatively few observations were used to train the model and in the presence of strong noise. The applications to real data showed a performance comparable, and sometimes slightly superior, to that of other ML methods used in previous studies, such as different types of neural networks and support vector machines.

PCE, however, offers several advantages. First, the framework performs well on very different tasks, with only little parameter tuning needed to adapt the methodology to the specific data considered. In fact, only the total degree p , the q -norm parameter and the interaction degree r are to be specified. As a single analysis takes only a few seconds to a minute to be completed on a standard laptop (depending on the size of the data), is straightforward to loop it on an array of (p, q, r) values, and to retain the PCE with minimum error in the end. This feature distinguishes PCE from the above mentioned ML methods, which instead are known to be highly sensitive to their hyperparameters and require an appropriate and typically time consuming calibration (Claesen and Moor, 2015). Indeed, it is worth noting that, in the comparisons we made, all PCE metamodels were built by using the very same procedure and hyperparameters (p, q, r) . When compared to the best NNs or SVM found in other studies, which differed significantly among each other in their construction and structure, the PCE metamodels exhibited a comparable performance.

Second, PCE delivers not only accurate pointwise predictions of the output for any given input, but also statistics thereof in the presence of input uncertainties. This is made possible by combining the PCE metamodel with a proper probabilistic characterization of the input uncertainties through marginal distributions and copulas. The methodology works well also in the presence of several inputs (as tested on problems of dimension up to 10) and of sample sets of comparably small size.

Third, the analytical expression of the output yielded by PCE in terms of a simple

polynomial of the input makes the model easy to interpret. For instance, its coefficients are directly related to the first and second moments of the output. For independent inputs, Sobol sensitivity indices are also directly encoded in the polynomial coefficients (Sudret, 2008). Sensitivity indices for dependent inputs (*e.g.*, Kucherenko et al. (2012)) may be computed numerically. Other statistics of the output, *e.g.*, its full PDF, can be efficiently estimated by resampling.

Fourth, the polynomial form makes the calibrated metamodel portable to embedded devices (*e.g.*, drones). For this kind of applications, the demonstrated robustness to noise in the data is a particularly beneficial feature.

Fifth and last, PCE needs relatively few data points to attain acceptable performance levels, as shown here on various test cases. This feature demonstrates the validity of PCE metamodeling for problems affected by data scarcity, also when combined with complex vine copula representations of the input dependencies.

One limitation of PCE-based regression as presented here is its difficulty in dealing with data of large size or consisting of a large number of inputs. Both features lead to a substantially increased computational cost needed to fit the PCE parameters and (if statistical estimation is wanted and the inputs are dependent) to infer the copula. Various solutions are possible. As for the PCE construction, in the presence of very large training sets the PCE may be initially trained on a subset of the available observations, and subsequently refined by enriching the training set with points in the region where the observed error is larger. Regarding copula inference, which is only needed for an accurate quantification of the prediction’s uncertainty, a possible solution is to employ a Gaussian copula. The latter involves a considerably faster fitting than the more complex vine copulas, and still yielded in our simulations acceptable performance. Alternatively, one may reduce the computational time needed for parameter estimation by parallel computing, as done in Wei et al. (2016).

Finally, the proposed methodology has been shown here on data characterized by continuous input variables only. PCE construction in the presence of discrete data is equally possible, and the Stiltjes orthogonalization procedure is known to be quite stable in that case (Gautschi, 1982). The a-posteriori quantification of the output uncertainty, however, generally poses a challenge. Indeed, it involves the inference of a copula among discrete random variables, which requires a different construction Genest and Nešlehová (2007). Recently, however, methods have been proposed to this end, including inference for R-vines (Panagiotelis et al., 2012, 2017). Further work is foreseen to integrate these advances with PCE metamodeling.

Acknowledgments

Emiliano Torre gratefully acknowledges financial support from RiskLab, Department of Mathematics, ETH Zurich and from the Risk Center of the ETH Zurich.

References

- Aas, K. (2016). Pair-copula constructions for financial applications: A review. *Econometrics* 4(4), 43.
- Aas, K., C. Czado, A. Frigessi, and H. Bakken (2009). Pair-copula constructions of multiple dependence. *Insurance: Mathematics and Economics* 44(2), 182–198.
- Applegate, D. L., R. E. Bixby, V. Chvátal, and W. J. Cook (2006). *The Traveling Salesman Problem: A Computational Study*. New Jersey: Princeton University Press.
- Bedford, T. and R. M. Cooke (2002). Vines – a new graphical model for dependent random variables. *The Annals of Statistics* 30(4), 1031–1068.
- Bishop, C. (2009). *Pattern recognition and machine learning*. Springer.
- Blatman, G. and B. Sudret (2011). Adaptive sparse polynomial chaos expansion based on Least Angle Regression. *J. Comput. Phys* 230, 2345–2367.
- Can, A. (1992). Specification and estimation of hedonic housing price models. *Regional Science and Urban Economics* 22(3), 453–474.
- Chan, S. and A. H. Elsheikh (2018). A machine learning approach for efficient uncertainty quantification using multiscale methods. *Journal of Computational Physics* 354, 493–511.
- Claesen, M. and B. D. Moor (2015). Hyperparameter search in machine learning. *arXiv 1502.02127*.
- Cortez, P., A. Cerdeira, F. Almeida, T. Matos, and J. Reis (2009). Modeling wine preferences by data mining from physicochemical properties. *Decision Support Systems* 47, 547–553.
- Czado, C. (2010). *Pair-Copula Constructions of Multivariate Copulas*, pp. 93–109. Berlin, Heidelberg: Springer Berlin Heidelberg.
- Dißmann, J., E. C. Brechmann, C. Czado, and D. Kurowicka (2013). Selecting and estimating regular vine copulae and application to financial returns. *Computational Statistics and Data Analysis* 59, 52–69.
- Efron, B., T. Hastie, I. Johnstone, and R. Tibshirani (2004). Least angle regression. *Annals of Statistics* 32, 407–499.
- Ernst, O. G., A. Mugler, H.-J. Starkloff, and E. Ullmann (2012). On the convergence of generalized polynomial chaos expansions. *ESAIM: M2AN* 46(2), 317–339.

- Forman, G. and I. Cohen (2004). Learning from little: Comparison of classifiers given little training. In J.-F. Boulicaut, F. Esposito, F. Giannotti, and D. Pedreschi (Eds.), *Knowledge Discovery in Databases: PKDD 2004*, Berlin, Heidelberg, pp. 161–172. Springer Berlin Heidelberg.
- Gautschi, W. (1982). On generating orthogonal polynomials. *SIAM J. Sci. Stat. Comput.* 3(3), 289–317.
- Genest, C. and J. Nešlehová (2007). A primer on copulas for count data. *The Astin Bulletin* 37, 475–515.
- Ghanem, R. and P.-D. Spanos (1990). Polynomial chaos in stochastic finite elements. *J. Applied Mech.* 57, 197–202.
- Gilley, O. W. and R. K. Pace (1995). Improving hedonic estimation with an inequality restricted estimator. *The Review of Economics and Statistics* 77(4), 609–621.
- Haff, I. H., K. Aas, and A. Frigessi (2010). On the simplified pair-copula construction – simply useful or too simplistic? *Journal of Multivariate Analysis* 101, 1296–1310.
- Harrison, D. and D. L. Rubinfeld (1978). Hedonic housing prices and the demand for clean air. *Journal of Environmental Economics and Management* 5, 81–102.
- Ishigami, T. and T. Homma (1990). An importance quantification technique in uncertainty analysis for computer models. In *Proc. ISUMA'90, First Int. Symp. Unc. Mod. An.*, pp. 398–403. University of Maryland.
- Joe, H. (1996). Families of m -variate distributions with given margins and $m(m - 1)/2$ bivariate dependence parameters. In L. Rüschendorf, B. Schweizer, and M. D. Taylor (Eds.), *Distributions with fixed marginals and related topics*, Volume 28 of *Lecture Notes–Monograph Series*, pp. 120–141. Institute of Mathematical Statistics.
- Joe, H. (Ed.) (2015). *Dependence modeling with copulas*. CRC Press.
- Kasiviswanathan, K. S., K. P. Sudheer, and J. He (2016). *Quantification of Prediction Uncertainty in Artificial Neural Network Models*, pp. 145–159. Cham: Springer International Publishing.
- Kirk, J. (2014). Traveling salesman problem – genetic algorithm.
<https://ch.mathworks.com/matlabcentral/fileexchange/13680-traveling-salesman-problem-genetic-algorithm>.
- Kucherenko, S., A. Tarantola, and P. Annoni (2012). Estimation of global sensitivity indices for models with dependent variables. *Comput. Phys. Comm.* 183, 937–946.

- Kurowicka, D. and R. M. Cooke (2005). Distribution-free continuous Bayesian belief nets. In A. Wilson, N. Limnios, S. Keller-McNulty, and Y. Armijo (Eds.), *Modern Statistical and Mathematical Methods in Reliability*, Chapter 10, pp. 309–322. World Scientific Publishing.
- Kurz, M. (2015). Vine copulas with matlab.
<https://ch.mathworks.com/matlabcentral/fileexchange/46412-vine-copulas-with-matlab>.
- Lebrun, R. and A. Dutfoy (2009). Do Rosenblatt and Nataf isoprobabilistic transformations really differ? *Prob. Eng. Mech.* *24*, 577–584.
- Lichman, M. (2013). UCI machine learning repository.
- Mentch, L. and G. Hooker (2016). Quantifying uncertainty in random forests via confidence intervals and hypothesis tests. *Journal of Machine Learning Research* *17*, 1–41.
- Morales-Nápoles, O. (2011). Counting vines. In D. Kurowicka and H. Joe (Eds.), *Dependence Modeling: Vine Copula Handbook*, Chapter 9, pp. 189–218. World Scientific Publisher Co.
- Nelsen, R. (2006). *An introduction to copulas* (Second ed.). Springer Series in Statistics. Springer-Verlag New York.
- Oladyshkin, S. and W. Nowak (2012). Data-driven uncertainty quantification using the arbitrary polynomial chaos expansion. *Reliability Engineering and System Safety* *106*, 179–190.
- Panagiotelis, A., C. Czado, and H. Joe (2012). Pair copula constructions for multivariate discrete data. *J. Amer. Statist. Assoc.* *107*, 1063–1072.
- Panagiotelis, A., C. Czado, H. Joe, and J. Stöber (2017). Model selection for discrete regular vine copulas. *Computational Statistics & Data Analysis* *106*, 138–152.
- Parzen, E. (1962). On estimation of a probability density function and mode. *The Annals of Mathematical Statistics* *33*(3), 1065–1076.
- Puig, B., F. Poirion, and C. Soize (2002). Non-Gaussian simulation using Hermite polynomial expansion: convergences. *Prob. Eng. Mech.* *17*, 253–264.
- Quinlan, J. R. (1993). Combining instance-based and model-based learning. In *Proceedings on the Tenth International Conference of Machine Learning*, pp. 236–243.
- R Kelley Pace, O. W. G. (1997). Using the spatial configuration of the data to improve estimation. *Journal of Real Estate Finance and Economics* *14*(3), 333–340.
- Rosenblatt, M. (1952). Remarks on a multivariate transformation. *The Annals of Mathematical Statistics* *23*, 470–472.

- Rosenblatt, M. (1956). Remarks on some nonparametric estimates of a density function. *The Annals of Mathematical Statistics* 27(3), 832–837.
- Saltelli, A., K. Chan, and E. Scott (Eds.) (2000). *Sensitivity analysis*. J. Wiley & Sons.
- Schepsmeier, U. (2015). Efficient information based goodness-of-fit tests for vine copula models with fixed margins. *Journal of Multivariate Analysis* 138(C), 34–52.
- Schölkopf, B. and A. Smola (2002). *Learning with kernels*. MIT Press.
- Sklar, A. (1959). Fonctions de répartition à n dimensions et leurs marges. *Publications de l'Institut de Statistique de L'Université de Paris* 8, 229–231.
- Snoek, J., H. Larochelle, and R. P. Adams (2012). Practical Bayesian optimization of machine learning algorithms. In *Proceedings of the 25th International Conference on Neural Information Processing Systems - Volume 2*, NIPS'12, USA, pp. 2951–2959. Curran Associates Inc.
- Sobol', I. (1993). Sensitivity estimates for nonlinear mathematical models. *Mathematical Modeling & Computational Experiment* 1, 407–414.
- Sobol', I. M. (1967). On the distribution of points in a cube and the approximate evaluation of integrals. *USSR Computational Mathematics and Mathematical Physics* 7(4), 86–112.
- Soize, C. and R. Ghanem (2004). Physical systems with random uncertainties: chaos representations with arbitrary probability measure. *SIAM J. Sci. Comput.* 26(2), 395–410.
- Stöber, J., H. Joe, and C. Czado (2013). Simplified pair copula constructions — limitations and extensions. *Journal of Multivariate Analysis* 119, 101–118.
- Stuart, A. and K. Ord (1994). *Kendall's advanced theory of statistics Vol. 1 – Distribution theory*. Arnold.
- Sudret, B. (2008). Global sensitivity analysis using polynomial chaos expansions. *Reliab. Eng. Sys. Safety* 93, 964–979.
- Sudret, B., S. Marelli, and C. Lataniotis (2015). Sparse polynomial chaos expansions as a machine learning regression technique. International Symposium on Big Data and Predictive Computational Modeling, invited lecture.
- Todor, R.-A. and C. Schwab (2007). Convergence rates for sparse chaos approximations of elliptic problems with stochastic coefficients. *IMA J. Numer. Anal* 27, 232–261.
- Torre, E., S. Marelli, P. Embrechts, and B. Sudret (2017). A general framework for data-driven uncertainty quantification under complex input dependencies using vine copulas. *arXiv 1709.08626*. Under revision in Probabilistic Engineering Mechanics.

- Tüfekci, P. (2014). Prediction of full load electrical power output of a base load operated combined cycle power plant using machine learning methods. *International Journal of Electrical Power & Energy Systems* 60, 126–140.
- Vapnik, V. (1995). *The Nature of Statistical Learning Theory*. Springer-Verlag, New York.
- Wan, X. and G. E. Karniadakis (2006). Beyond Wiener-Askey expansions: handling arbitrary PDFs. *J. Sci. Comput.* 27, 455–464.
- Wei, Z., D. Kim, and E. M. Conlon (2016). Parallel computing for copula parameter estimation with big data: A simulation study. *arXiv 1609.05530*.
- Witten, I. H., E. Frank, M. A. Hall, and C. J. Pal (2016). *Data Mining, Fourth Edition: Practical Machine Learning Tools and Techniques* (4th ed.). San Francisco, CA, USA: Morgan Kaufmann Publishers Inc.
- Xiu, D. and G. Karniadakis (2002). The Wiener-Askey polynomial chaos for stochastic differential equations. *SIAM J. Sci. Comput.* 24(2), 619–644.

A Mutually dependent inputs modelled through copulas

In Section 2.3 we illustrated PCE for an input \mathbf{Z} with independent components being uniformly distributed in $[0, 1]$. \mathbf{Z} was obtained from the true input \mathbf{X} by assuming either that the latter had independent components as well, and thus defining $Z_i = F_i(X_i)$, or that a transformation \mathcal{T} to perform this mapping was available.

This section recalls known results in probability theory allowing one to specify $F_{\mathbf{X}}$ in terms of its marginal distributions and a dependence function called the *copula* of \mathbf{X} . We focus in particular on regular vine copulas (R-vines), for which the transformation \mathcal{T} can be computed numerically. R-vines provide a flexible class of dependence models for $f_{\mathbf{X}}$. This will prove beneficial to the ability of the PCE models to predict statistics of the output accurately, compared to simpler dependence models. However, and perhaps counter-intuitively, the pointwise error may not decrease accordingly (see Section 2.1 for details), especially when \mathcal{T} is highly non-linear. Examples on simulated data and a discussion are provided in Section 3.

A.1 Copulas and Sklar’s theorem

A d -copula is defined as a d -variate joint CDF $C : [0, 1]^d \rightarrow [0, 1]$ with uniform marginals in the unit interval, that is,

$$C(1, \dots, 1, u_i, 1, \dots, 1) = u_i \quad \forall u_i \in [0, 1], \quad \forall i = 1, \dots, d.$$

Sklar's theorem (Sklar, 1959) guarantees that any d -variate joint CDF can be expressed in terms of d marginals and a copula, specified separately.

Theorem (Sklar). *For any d -variate CDF $F_{\mathbf{X}}$ with marginals F_1, \dots, F_d , a d -copula $C_{\mathbf{X}}$ exists, such that*

$$F_{\mathbf{X}}(\mathbf{x}) = C_{\mathbf{X}}(F_1(x_1), F_2(x_2), \dots, F_d(x_d)). \quad (\text{A.1})$$

Besides, $C_{\mathbf{X}}$ is unique on $\text{Ran}(F_1) \times \dots \times \text{Ran}(F_d)$, where Ran is the range operator. In particular, $C_{\mathbf{X}}$ is unique on $[0, 1]^d$ if all F_i are continuous, and it is given by

$$C_{\mathbf{X}}(u_1, u_2, \dots, u_d) = F_{\mathbf{X}}(F_1^{-1}(u_1), F_2^{-1}(u_2), \dots, F_d^{-1}(u_d)). \quad (\text{A.2})$$

Conversely, for any d -copula C and any set of d univariate CDFs F_i , $i = 1, \dots, d$, the function $F : \mathbb{R}^d \rightarrow [0, 1]$ defined by

$$F(x_1, x_2, \dots, x_d) := C(F_1(x_1), F_2(x_2), \dots, F_d(x_d)) \quad (\text{A.3})$$

is a d -variate CDF with marginals F_1, \dots, F_d .

Throughout this study it is assumed that $F_{\mathbf{X}}$ has continuous marginals F_i . The relation (A.3) allows one to model any multivariate CDF F by modelling separately d univariate CDFs F_i and a copula function C . One first models the marginals F_i , then transforms each X_i into a uniform random variable $U_i = F_i(X_i)$ by the so-called probability integral transform (PIT)

$$\mathcal{T}^{\text{PIT}} : \mathbf{X} \mapsto \mathbf{U} = (F_1(X_1), \dots, F_M(X_M))^{\top}. \quad (\text{A.4})$$

Finally, the copula C of \mathbf{X} is obtained as the joint CDF of \mathbf{U} . The copula models the dependence properties of the random vector. For instance, mutual independence is achieved by using the independence copula

$$C(\mathbf{u}) = \prod_{i=1}^d u_i. \quad (\text{A.5})$$

Table A.4 provides a list of 19 different parametric families of pair copulas implemented in the VineCopulaMatlab toolbox (Kurz, 2015), which was also used in this study. Details on copula theory and on various copula families can be found in Nelsen (2006) and in Joe (2015).

Sklar's theorem can be re-stated in terms of probability densities. If \mathbf{X} admits joint PDF $f_{\mathbf{X}}(\mathbf{x}) := \frac{\partial^d F_{\mathbf{X}}(\mathbf{x})}{\partial x_1 \dots \partial x_M}$ and copula density $c_{\mathbf{X}}(\mathbf{u}) := \frac{\partial^d C_{\mathbf{X}}(\mathbf{u})}{\partial u_1 \dots \partial u_M}$, $\mathbf{u} \in [0, 1]^d$, then

$$f_{\mathbf{X}}(\mathbf{x}) = c(F_1(x_1), F_2(x_2), \dots, F_d(x_d)) \cdot \prod_{i=1}^d f_i(x_i). \quad (\text{A.6})$$

Once all marginal PDFs f_i and the corresponding CDFs F_i have been determined (see Section 2.3.2), each data point $\mathbf{x}^{(j)} \in \mathcal{X}$ is mapped onto the unit hypercube by the PIT (A.4), obtaining a transformed data set \mathbf{U} of *pseudo-observations* of \mathbf{U} . The copula of \mathbf{X} can then be inferred on \mathbf{U} .

A.2 Vine copulas

In high dimension d , specifying a d -copula which properly describes all pairwise and higher-order input dependencies may be challenging. Multivariate extensions of pair-copula families (e.g. Gaussian or Archimedean copulas) are often inadequate when d is large. In Joe (1996) and later in Bedford and Cooke (2002) and Aas et al. (2009), an alternative construction by multiplication of 2-copulas was introduced. Copula models built in this way are called *vine copulas*. Here we briefly introduce the vine copula formalism, referring to the references for details.

Let $\mathbf{u}_{\bar{i}}$ be the vector obtained from the vector \mathbf{u} by removing its i -th component, *i.e.*, $\mathbf{u}_{\bar{i}} = (u_1, \dots, u_{i-1}, u_{i+1}, \dots, u_d)^\top$. Similarly, let $\mathbf{u}_{\overline{\{i,j\}}}$ be the vector obtained by removing the i -th and j -th component, and so on. For a general subset $\mathcal{A} \subset \{1, \dots, d\}$, $\mathbf{u}_{\overline{\mathcal{A}}}$ is defined analogously. Also, $F_{\overline{\mathcal{A}}|\mathcal{A}}$ and $f_{\overline{\mathcal{A}}|\mathcal{A}}$ indicate in the following the joint CDF and PDF of the random vector $\mathbf{X}_{\overline{\mathcal{A}}}$ conditioned on $\mathbf{X}_{\mathcal{A}}$. In the following, $\mathcal{A} = \{i_1, \dots, i_k\}$ and $\overline{\mathcal{A}} = \{j_1, \dots, j_l\}$ form a partition of $\{1, \dots, d\}$, *i.e.*, $\mathcal{A} \cup \overline{\mathcal{A}} = \{1, \dots, d\}$ and $\mathcal{A} \cap \overline{\mathcal{A}} = \emptyset$.

Using (A.6), $f_{\overline{\mathcal{A}}|\mathcal{A}}$ can be expressed as

$$\begin{aligned} f_{\overline{\mathcal{A}}|\mathcal{A}}(\mathbf{x}_{\overline{\mathcal{A}}}|\mathbf{x}_{\mathcal{A}}) &= c_{\overline{\mathcal{A}}|\mathcal{A}}(F_{j_1|\mathcal{A}}(x_{j_1}|\mathbf{x}_{\mathcal{A}}), F_{j_2|\mathcal{A}}(x_{j_2}|\mathbf{x}_{\mathcal{A}}), \dots, F_{j_l|\mathcal{A}}(x_{j_l}|\mathbf{x}_{\mathcal{A}})) \times \\ &\quad \times \prod_{j \in \overline{\mathcal{A}}} f_{j|\mathcal{A}}(x_j|\mathbf{x}_{\mathcal{A}}), \end{aligned} \quad (\text{A.7})$$

where $c_{\overline{\mathcal{A}}|\mathcal{A}}$ is an l -copula density – that of the conditional random variables $(X_{j_1|\mathcal{A}}, X_{j_2|\mathcal{A}}, \dots, X_{j_l|\mathcal{A}})^\top$ – and $f_{j|\mathcal{A}}$ is the conditional PDF of X_j given $\mathbf{X}_{\mathcal{A}}$, $j \in \overline{\mathcal{A}}$. Following Joe (1996), the univariate conditional distributions $F_{j|\mathcal{A}}$ can be further expressed in terms of any conditional pair copula $C_{ji|\mathcal{A} \setminus \{i\}}$ between $X_{j|\mathcal{A} \setminus \{i\}}$ and $X_{i|\mathcal{A} \setminus \{i\}}$, $i \in \mathcal{A}$:

$$F_{j|\mathcal{A}}(x_j|\mathbf{x}_{\mathcal{A}}) = \frac{\partial C_{ji|\mathcal{A} \setminus \{i\}}(u_j, u_i)}{\partial u_i} \Big|_{(F_{j|\mathcal{A} \setminus \{i\}}(x_j|\mathbf{x}_{\mathcal{A} \setminus \{i\}}), F_{i|\mathcal{A} \setminus \{i\}}(x_i|\mathbf{x}_{\mathcal{A} \setminus \{i\}}))}. \quad (\text{A.8})$$

An analogous relation readily follows for conditional densities:

$$\begin{aligned} f_{j|\mathcal{A}}(x_j|\mathbf{x}_{\mathcal{A}}) &= \frac{\partial F_{j|\mathcal{A}}(x_j|\mathbf{x}_{\mathcal{A}})}{\partial x_j} \\ &= c_{ji|\mathcal{A} \setminus \{i\}}(F_{j|\mathcal{A} \setminus \{i\}}(x_j|\mathbf{x}_{\mathcal{A} \setminus \{i\}}), F_{i|\mathcal{A} \setminus \{i\}}(x_i|\mathbf{x}_{\mathcal{A} \setminus \{i\}})) \times \\ &\quad \times f_{j|\mathcal{A} \setminus \{i\}}(x_j|\mathbf{x}_{\mathcal{A} \setminus \{i\}}). \end{aligned} \quad (\text{A.9})$$

Substituting iteratively (A.8)-(A.9) into (A.7), Bedford and Cooke (2002) expressed $f_{\mathbf{X}}$ as a product of pair copula densities multiplied by $\prod_i f_i$. Recalling (A.6), it readily follows that the associated joint copula density c can be factorised into pair copula densities. Copulas expressed in this way are called vine copulas.

The factorisation is not unique: the pair copulas involved in the construction depend on the variables chosen in the conditioning equations (A.8)-(A.9) at each iteration. To organise them, Bedford and Cooke (2002) introduced a graphical model called the regular vine (R-vine). An R-vine among d random variables is represented by a graph consisting of $d - 1$

trees T_1, T_2, \dots, T_{d-1} , where each tree T_i consists of a set N_i of nodes and a set E_i of edges $e = (j, k)$ between nodes j and k . The trees T_i satisfy the following three conditions:

1. Tree T_1 has nodes $N_1 = \{1, \dots, d\}$ and $d - 1$ edges E_1
2. for $i = 2, \dots, d - 1$, the nodes of T_i are the edges of T_{i-1} : $N_i = E_{i-1}$
3. Two edges in tree T_i can be joined as nodes of tree T_{i+1} by an edge only if they share a common node in T_i (proximity condition)

To build an R-vine with nodes $\mathcal{N} = \{N_1, \dots, N_{d-1}\}$ and edges $\mathcal{E} = \{E_1, \dots, E_{d-1}\}$, one defines for each edge e linking nodes $j = j(e)$ and $k = k(e)$ in tree T_i , the sets $I(e)$ and $D(e)$ as follows:

- If $e \in E_1$ (edge of tree T_1), then $I(e) = \{j, k\}$ and $D(e) = \emptyset$,
- If $e \in E_i, i \geq 2$, then $D(e) = D(j) \cup D(k) \cup (I(j) \cap I(k))$ and $I(e) = (I(j) \cup I(k)) \setminus D(e)$.

$I(e)$ contains always two indices j_e and k_e , while $D(e)$ contains $i - 1$ indices for $e \in E_i$. One then associates each edge e with the conditional pair copula $C_{j_e, k_e | D(e)}$ between X_{j_e} and X_{k_e} conditioned on the variables with indices in $D(e)$. An R-vine copula density with d nodes can thus be expressed as Aas (2016)

$$c(\mathbf{u}) = \prod_{i=1}^{d-1} \prod_{e \in E_i} c_{j_e, k_e | D(e)}(u_{j_e | D(e)}, u_{k_e | D(e)}). \quad (\text{A.10})$$

Two special classes of R-vines are the drawable vine (D-vine; (Kurowicka and Cooke, 2005)) and the canonical vine (C-vine; Aas et al. (2009)). Denoting $F(x_i) = u_i$ and $F_{i|\mathcal{A}}(x_i | \mathbf{x}_{\mathcal{A}}) = u_{i|\mathcal{A}}, i \notin \mathcal{A}$, a C-vine density is given by the expression

$$c(\mathbf{u}) = \prod_{j=1}^{d-1} \prod_{i=1}^{d-j} c_{j, j+i | \{1, \dots, j-1\}}(u_{j | \{1, \dots, j-1\}}, u_{j+i | \{1, \dots, j-1\}}), \quad (\text{A.11})$$

while a D-vine density is expressed by

$$c(\mathbf{u}) = \prod_{j=1}^{d-1} \prod_{i=1}^{d-j} c_{i, i+j | \{i+1, \dots, i+j-1\}}(u_{i | \{i+1, \dots, i+j-1\}}, u_{i+j | \{i+1, \dots, i+j-1\}}). \quad (\text{A.12})$$

The graphs associated to a 5-dimensional C-vine and to a 5-dimensional D-vine are shown in Figure 13. Note that this simplified illustration differs from the standard one introduced in Aas et al. (2009) and commonly used in the literature.

A.3 Vine copula inference in practice

We consider the purely data-driven case, typical in machine learning applications, where \mathbf{X} is only known through a set \mathcal{X} of independent observations. As remarked in Section 2.3.2, inference on $C_{\mathbf{X}}$ can be performed on \mathbf{U} , obtained from \mathcal{X} by probability integral transform of each component after the marginals f_i have been assigned. In this setup, building a vine copula model on \mathbf{U} involves the following steps:

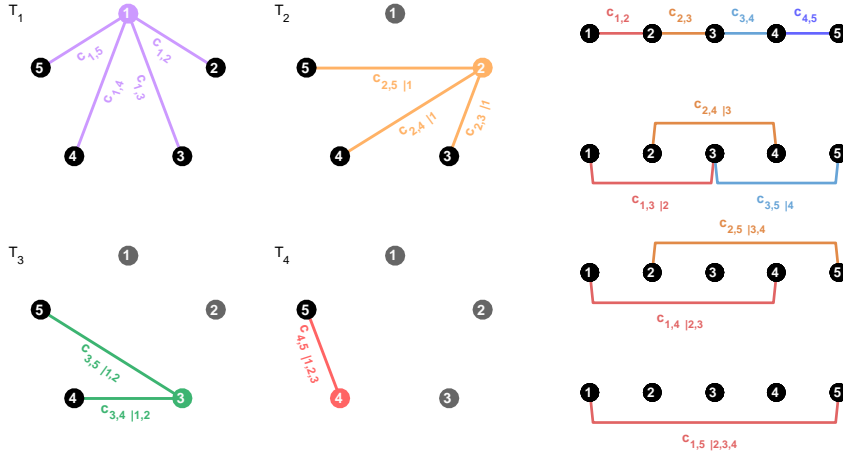


Figure 13: **Graphical representation of C- and D-vines.** The pair copulas in each tree of a 5-dimensional C-vine (left; conditioning variables are shown in grey) and of a 5-dimensional D-vine (right; conditioning variables are those between the connected nodes).

1. Selecting a vine structure (for C- and D-vines: selecting the order of the nodes);
2. Selecting the parametric family of each pair copula;
3. Fitting the pair copula parameters to \mathbf{u} .

Steps 1-2 form the representation problem. Concerning step 3, algorithms to compute the likelihood of C- and D-vines (Aas et al., 2009) and of R-vines (Joe, 2015) given a data set \mathbf{u} exist, enabling parameter fitting based on maximum likelihood. In principle, the vine copula that best fits the data may be determined by iterating the maximum fitting approach over all possible vine structures and all possible parametric families of comprising pair copulas. In practice however, this approach is computationally infeasible in even moderate dimension d due to the large number of possible structures (Morales-Nápoles, 2011) and of pair copulas comprising the vine.

Taking a different approach first suggested in Aas et al. (2009) and common to many applied studies, we first solve step 1 separately. The optimal vine structure is selected heuristically so as to capture first the pairs (X_i, X_j) with the strongest dependence (which then fall in the upper trees of the vine). The Kendall's tau (Stuart and Ord, 1994) is selected as such a measure of dependence, defined by

$$\tau_{ij} = \mathbb{P}((X_i - \tilde{X}_i)(X_j - \tilde{X}_j) > 0) - \mathbb{P}((X_i - \tilde{X}_i)(X_j - \tilde{X}_j) < 0), \quad (\text{A.13})$$

where $(\tilde{X}_i, \tilde{X}_j)$ is an independent copy of (X_i, X_j) . If the copula of (X_i, X_j) is C_{ij} , then

$$\tau_K(X_i, X_j) = 4 \int \int_{[0,1]^2} C_{ij}(u, v) dC_{ij}(u, v) - 1. \quad (\text{A.14})$$

For a C-vine, ordering the variables X_1, \dots, X_M in decreasing order of dependence strength corresponds to select the central node in tree T_1 as the variable X_{i_1} which maximises

$\sum_{j \neq i_1} \tau_{i_1 j}$, then the node of tree T_2 as the variable X_{i_2} which maximises $\sum_{j \notin \{i_1, i_2\}} \tau_{i_2 j}$, and so on. For a D-vine, this means ordering the variables $X_{i_1}, X_{i_2}, \dots, X_{i_d}$ in the first tree so as to maximise $\sum_{k=1}^{d-1} \tau_{i_k i_{k+1}}$, which we solve as an open travelling salesman problem (OTSP) (Applegate et al., 2006). An open source Matlab implementation of a genetic algorithm to solve the OTSP is provided in Kirk (2014). An algorithm to find the optimal structure for R-vines has been proposed in Dißmann et al. (2013).

For a selected vine structure, the vine copula with that structure that best fits the data is inferred by iterating, for each pair copula forming the vine, steps 2 and 3 over a list of pre-defined parametric families and their rotated versions. The families considered for inference in this paper are listed in Table A.4. The rotations of a pair copula C by 90, 180 and 270 degrees are defined, respectively, by

$$\begin{aligned} C^{(90)}(u, v) &= v - C(1 - u, v), \\ C^{(180)}(u, v) &= u + v - 1 + C(1 - u, 1 - v), \\ C^{(270)}(u, v) &= u - C(u, 1 - v). \end{aligned} \tag{A.15}$$

(Note that $C^{(90)}$ and $C^{(270)}$ are obtained by flipping the copula density c around the horizontal and vertical axis, respectively; some references provide the formulas for actual rotations: $C^{(90)}(u, v) = v - C(v, 1 - u)$, $C^{(270)}(u, v) = u - C(1 - v, u)$). Including the rotated copulas, 62 families were considered in total for inference in our study.

To facilitate inference, we rely on the so-called *simplifying assumption* commonly adopted for vine copulas, namely that the pair copulas $C_{j(e), k(e)|D(e)}$ in (A.10) only depend on the variables with indices in $D(e)$ through the arguments $F_{i(e)|D(e)}$ and $F_{j(e)|D(e)}$ (Czado, 2010). While being exact only in particular cases, this assumption is usually not severe (Haff et al., 2010). Estimation techniques for non-simplified vine models have also been proposed (Stöber et al., 2013).

For each pair copula composing the vine, its parametric family is selected as the family that minimises the Akaike information criterion (AIC)

$$\text{AIC} = 2 \times (k - \log L), \tag{A.16}$$

where k is the number of parameters of the pair copula and $\log L$ is its log-likelihood. The process is iterated over all pair copulas forming the vine, starting from the unconditional copulas in the top tree (sequential inference). Finally (and optionally), one keeps the vine structure and the copula families obtained in this way (that is, the parametric form of the vine), and performs global likelihood maximisation.

A.4 Rosenblatt transform of R-vines

Suppose that the probabilistic input model $F_{\mathbf{X}}$ is specified in terms of marginals F_i and a copula $C_{\mathbf{X}}$, the polynomial chaos representation can be more conveniently achieved by first mapping \mathbf{X} onto a vector $\mathbf{Z} = \mathcal{T}(\mathbf{X})$ with independent components.

ID	Name	CDF	Parameter range
1	AMH	$\frac{uv}{1 - \theta(1-u)(1-v)}$	$\theta \in [-1, 1]$
2	AsymFGM	$uv(1 + \theta(1-u)^2v(1-v))$	$\theta \in [0, 1]$
3	BB1	$\left(1 + \left((u^{-\theta_2} - 1)^{\theta_1} + (v^{-\theta_2} - 1)^{\theta_1}\right)^{1/\theta_1}\right)^{-1/\theta_2}$	$\theta_1 \geq 1, \theta_2 > 0$
4	BB6	$1 - \left(1 - \exp\left\{-\left[(-\log(1 - (1-u)^{\theta_2}))^{\theta_1} + (-\log(1 - (1-v)^{\theta_2}))^{\theta_1}\right]^{1/\theta_1}\right\}\right)^{1/\theta_2}$	$\theta_1 \geq 1, \theta_2 \geq 1$
5	BB7	$\varphi(\varphi^{-1}(u) + \varphi^{-1}(v))$, where $\varphi(w) = \varphi(w; \theta_1, \theta_2) = 1 - (1 - (1+w)^{-1/\theta_1})^{1/\theta_2}$	$\theta_1 \geq 1, \theta_2 > 0$
6	BB8	$\frac{1}{\theta_1} \left(1 - \left(1 - \frac{(1 - (1 - \theta_1 u)^{\theta_2})(1 - (1 - \theta_1 v)^{\theta_2})}{1 - (1 - \theta_1)^{\theta_2}}\right)^{1/\theta_2}\right)$	$\theta_1 \geq 1, \theta_2 \in (0, 1]$
7	Clayton	$(u^{-\theta} + v^{-\theta} - 1)^{-1/\theta}$	$\theta > 0$
8	FGM	$uv(1 + \theta(1-u)(1-v))$	$\theta \in (-1, 1)$
9	Frank	$-\frac{1}{\theta} \log\left(\frac{1 - e^{-\theta} - (1 - e^{-\theta u})(1 - e^{-\theta v})}{1 - e^{-\theta}}\right)$	$\theta \in \mathbb{R} \setminus \{0\}$
10	Gaussian	$\Phi_{2,\theta}(\Phi^{-1}(u), \Phi^{-1}(v))$ ^(a)	$\theta \in (-1, 1)$
11	Gumbel	$\exp(-((-\log u)^\theta + (-\log v)^\theta)^{1/\theta})$	$\theta \in [1, +\infty)$
12	Iterated FGM	$uv(1 + \theta_1(1-u)(1-v) + \theta_2uv(1-u)(1-v))$	$\theta_1, \theta_2 \in (-1, 1)$
13	Joe/B5	$1 - ((1-u)^\theta + (1-v)^\theta + (1-u)^\theta(1-v)^\theta)^{1/\theta}$	$\theta \geq 1$
14	Partial Frank	$\frac{uv}{\theta(u+v-uv)}(\log(1 + (e^{-\theta} - 1)(1 + uv - u - v)) + \theta)$	$\theta > 0$
15	Plackett	$\frac{1 + (\theta - 1)(u + v) - \sqrt{(1 + (\theta - 1)(u + v))^2 - 4\theta(\theta - 1)uv}}{2(\theta - 1)}$	$\theta \geq 0$
16	Tawn-1	$(uv)^{A\left(\frac{\log v}{\log(uv)}; \theta_1, \theta_3\right)}$, where $A(w; \theta_1, \theta_3) = (1 - \theta_3)w + [w^{\theta_1} + (\theta_3(1-w))^{\theta_1}]^{1/\theta_1}$	$\theta_1 \geq 1, \theta_3 \in [0, 1]$
17	Tawn-2	$(uv)^{A\left(\frac{\log v}{\log(uv)}; \theta_1, \theta_2\right)}$, where $A(w; \theta_1, \theta_2) = (1 - \theta_2)(1-w) + [(\theta_2 w)^{\theta_1} + ((1-w))^{\theta_1}]^{1/\theta_1}$	$\theta_1 \geq 1, \theta_2 \in [0, 1]$
18	Tawn	$(uv)^{A(w; \theta_1, \theta_2, \theta_3)}$, where $w = \frac{\log v}{\log(uv)}$ and $A(w; \theta_1, \theta_2, \theta_3) = (1 - \theta_2)(1-w) + (1 - \theta_3)w + [(\theta_2 w)^{\theta_1} + (\theta_3(1-w))^{\theta_1}]^{1/\theta_1}$	$\theta_1 \geq 1, \theta_2, \theta_3 \in [0, 1]$
19	t-	$t_{2;\nu,\theta}(t_\nu^{-1}(u), t_\nu^{-1}(v))$ ^(b)	$\nu > 1, \theta \in (-1, 1)$

Table A.4: **Distributions of bivariate copula families used in vine inference.** Copula IDs (reported as assigned in the VineCopulaMatlab toolbox), distributions, and parameter ranges. (a) Φ is the univariate standard normal distribution, and $\Phi_{2;\theta}$ is the bivariate normal distribution with zero means, unit variances and correlation parameter θ . (b) t_ν is the univariate t distribution with ν degrees of freedom, and $t_{\nu,\theta}$ is the bivariate t distribution with ν degrees of freedom and correlation parameter θ .

The most general map \mathcal{T} of a random vector \mathbf{X} with dependent components onto a random vector \mathbf{Z} with mutually independent components is the Rosenblatt transform (Rosenblatt, 1952)

$$\mathcal{T} : \mathbf{X} \mapsto \mathbf{W}, \text{ where } \begin{cases} Z_1 = F_1(X_1) \\ Z_2 = F_{2|1}(X_2|X_1) \\ \vdots \\ Z_d = F_{d|1,\dots,d-1}(X_d|X_1, \dots, X_{d-1}) \end{cases} . \quad (\text{A.17})$$

One can rewrite (see also Lebrun and Dutfoy (2009)) $\mathcal{T} = \mathcal{T}^{(\Pi)} \circ \mathcal{T}^{\text{PIT}} : \mathbf{X} \mapsto \mathbf{U} \mapsto \mathbf{Z}$, where \mathcal{T}^{PIT} , given by (A.4), is known once the marginals have been computed, while $\mathcal{T}^{(\Pi)}$ is given by

$$\mathcal{T}^{(\Pi)} : \mathbf{U} \mapsto \mathbf{Z}, \text{ with } Z_i = C_{i|1,\dots,i-1}(U_i|U_1, \dots, U_{i-1}). \quad (\text{A.18})$$

Here, $C_{i|1,\dots,i-1}$ are conditional copulas of \mathbf{X} (and therefore of \mathbf{U}), obtained from $C_{\mathbf{X}}$ by differentiation. The variables Z_i are mutually independent and have marginal uniform distributions in $[0, 1]$. The problem of obtaining an isoprobabilistic transform of \mathbf{X} is hence reduced to the problem of computing derivatives of $C_{\mathbf{X}}$.

Representing $C_{\mathbf{X}}$ as an R-vine solves this problem. Indeed, algorithms to compute (A.18) have been established (see Schepsmeier (2015), and Aas et al. (2009) for algorithms specific to C- and D-vines). Given the pair-copulas C_{ij} in the first tree of the vine, the algorithms first compute their derivatives $C_{i|j}$. Higher-order derivatives $C_{i|ijk}, C_{i|ijkh}, \dots$ are obtained from the lower-order ones by inversion and differentiation. Derivatives and inverses of continuous pair copulas are generally computationally cheap to compute numerically, when analytical solutions are not available. The algorithms can be trivially implemented such that n sample points are processed in parallel.

B PCE with R-vine input models

If the inputs \mathbf{X} to the system are assumed to be mutually dependent, a possible approach to build a basis of orthogonal polynomials by tensor product is to transform \mathbf{X} into a random vector \mathbf{Z} with mutually independent components. The PCE metamodel can be built afterwards from \mathbf{Z} to Y . This approach, indicated by *lPCEonZ* in the text, comprises the following steps:

1. Model the joint CDF $F_{\mathbf{X}}$ of the input by inferring its marginals and copula. Specifically:
 - (a) infer the marginal CDFs $F_i, i = 1, \dots, d$, from the input observations \mathcal{X} (*e.g.*, by KDE);
 - (b) map \mathcal{X} onto $\mathbf{U} = \{\mathcal{T}^{\text{PIT}}(\hat{\mathbf{x}}^{(j)}), j = 1, \dots, n\} \subset [0, 1]^d$ by (A.4);
 - (c) model the copula $C_{\mathbf{X}} \equiv C_{\mathbf{U}}$ of the input by inference on \mathbf{U} ; R-vine copulas are compatible with this framework;

- (d) define $F_{\mathbf{X}}$ from the F_i and $C_{\mathbf{X}}$ using (A.1).
2. Map \mathbf{U} onto $\mathbf{Z} = \{\mathcal{T}^{(\Pi)}(\hat{\mathbf{u}}^{(j)}) \mid j = 1, \dots, n\}$ by the Rosenblatt transform (A.18). If the inferred marginals and copula are accurate, the underlying random vector \mathbf{Z} has approximately independent components, uniformly distributed in $[0, 1]$.
 3. Build a PCE metamodel on the training set $(\mathbf{Z}, \mathcal{Y})$. Specifically, obtain the basis of d -variate orthogonal polynomials by tensor product of univariate ones. The procedure used to build each i -th univariate basis depends on the distribution assigned to Z_i (if $Z_i \sim U([0, 1])$, use Legendre polynomials; if $Z_i \sim \hat{F}_i$ obtained by KDE, use arbitrary PCE).

The PCE metamodel obtained on the transformed input $\mathbf{Z} = \mathcal{T}(\mathbf{X})$ can be seen as a transformation of \mathbf{X} ,

$$Y_{\text{PC}}(\mathbf{Z}) = (Y_{\text{PC}} \circ \mathcal{T})(\mathbf{X}). \quad (\text{B.1})$$